HEATLINE ANALYSIS FOR MIXED CONVECTION FLOW OF NANOFLUID WITHIN A DRIVEN CAVITY CONTAINING HEAT GENERATING BLOCK
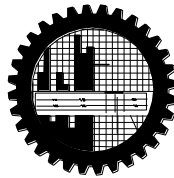
by

Ayesha Siddiqua

Student No. 0413093007P

Registration No. 0413093007, Session: April- 2013
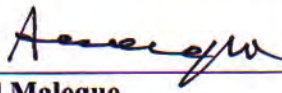
MASTER OF PHILOSOPHY
IN
MATHEMATICS

Department of Mathematics

BANGLADESH UNIVERSITY OF ENGINEERING AND

TECHNOLOGY, DHAKA-1000

March - 2018

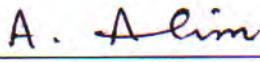The thesis entitled **"HEATLINE ANALYSIS FOR MIXED CONVECTION FLOW OF NANOFLUID WITHIN A DRIVEN CAVITY CONTAINING HEAT GENERATING BLOCK"**, submitted by **Ayesha Siddiqua**, Roll no: 0413093007P, Registration No. 0413093007, Session April-2013 has been accepted as satisfactory in partial fulfillment of the requirement for the degree of Master of Philosophy in Mathematics on 27 March 2018.

Board of Examiners
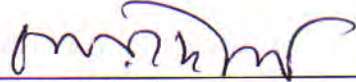
1. _____

   Dr. Salma Parvin
   Professor
   Department of Mathematics, BUET, Dhaka.

   Chairman
   (Supervisor)

2. _____

   Head
   Department of Mathematics, BUET, Dhaka.

   Member (Ex-Officio)

3. _____

   Dr. Md. Abdul Maleque
   Professor
   Department of Mathematics, BUET, Dhaka.

   Member

4. _____

   Dr. Md. Abdul Alim
   Professor
   Department of Mathematics, BUET, Dhaka.

   Member

5. _____

   Dr. Nazma Parveen
   Professor
   Department of Mathematics, BUET, Dhaka.

   Member

6. _____

   Dr. Mohammad Ferdows
   Associate Professor
   Department of Mathematics
   University of Dhaka, Dhaka-1000.

   Member (External)

CANDIDATE'S DECLARATION

I hereby announce that the work which is being presented in this thesis entitled 'HEATLINE ANALYSIS FOR MIXED CONVECTION FLOW OF NANOFLUID WITHIN A DRIVEN CAVITY CONTAINING HEAT GENERATING BLOCK' submitted in partial fulfillment of the requirements for the decoration of **Master of Philosophy** in Mathematics on March 2018, Bangladesh University of Engineering and Technology, Dhaka-1000 is my own work with proper citation and acknowledgement.

It is hereby declared that this thesis or any part of it has not been submitted elsewhere for any degree or diploma.

Ayesha Siddiqua
M. Phil Student
Department of Mathematics
March 2018

CERTIFICATE OF RESEARCH

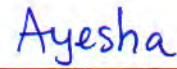This is to certify that the work presented in this thesis is carried out by the author under the supervision of **Dr. Salma Parvin**, Professor, Department of Mathematics, Bangladesh University of Engineering and Technology, Dhaka-1000.

Dr. Salma Parvin

Supervisor

Department of Mathematics

Bangladesh University of Engineering

and Technology (BUET)

Ayesha Siddiqua

DEDICATED TO MY FAMILY

ACKNOWLEDGEMENT

ABSTRACT

Heat transfer enhancement in presence of nanofluid by the effect of mixed convection in a lid driven cavity are often encountered in engineering systems which has been studied numerically. A Cartesian co-ordinate system is used with the origin at the lower left corner of the computational domain. The system consists of a double lid driven cavity with a heat generating object centered at the origin. Upper and lower lids are kept adiabatic. Two cases are considered, for case I left and right lids are moving in upward direction while for case II upper and lower lids are moving in opposite direction. The governing equations are solved by employing a finite-element method based on Galerkin weighted residuals. The investigations are conducted for different values of Reynolds number, solid fluid thermal conductivity ratio, Richardson number, heat generation parameter and solid volume fraction. Streamlines, isotherms, heatlines and heat transfer rate in terms of the average Nusselt number (Nu_{av}), average temperature (θ_{av}), maximum temperature, and the average heat flux magnitude for two above mentioned cases are presented for the aforesaid parameters. The results indicate that the mentioned parameters strongly affect the flow phenomenon and temperature field inside the cavity. Comparisons with previously published work are performed and the results are found to be in excellent agreement.

TABLE OF CONTENTS

NOMENCLATURE

c_p specific heat at constant pressure (J/kg.K)

g gravitational acceleration (ms^{-2})

h   convective heat transfer coefficient (W/m^2.K)

k thermal conductivity of fluid ($Wm^{-1}K^{-1}$)

L length of the cavity (m)

n dimensional distance either along x or y direction (m)

N non-dimensional distance either along X or Y direction

$N\alpha$ quadratic shape function

Nu   Nusselt number

p pressure

P non-dimensional pressure

Pr   Prandtl number

Re   Reynolds number

Ri   Richardson number

S_x surface tractions along X-axis

S_y surface tractions along Y-axis

T dimensional fluid temperature (K)

ΔT dimensional temperature difference (K)

u velocity in x-direction (m/s)

U dimensionless horizontal velocity

v velocity in y-direction (m/s)

V dimensionless vertical velocity

$\overline{A}$ cavity area (m^2)

x, y Cartesian coordinates (m)

X, Y   dimensionless Cartesian coordinates

Greek symbols

α	thermal diffusivity (m^2s^{-1})
β	coefficient of thermal expansion (K^{-1})
θ	dimensionless fluid temperature
$\Delta\theta$	dimensionless temperature difference
ψ	stream function
χ	solid volume fraction
Π	heat function
μ	dynamic viscosity of the fluid (m^2s^{-1})
ν	kinematic viscosity of the fluid (m^2s^{-1})
ρ	density of the fluid (kgm^{-3})

Subscripts

av	average
f	fluid
h	heated wall
nf	nanofluid
p	solid nanoparticle
s	solid

LIST OF TABLES

LIST OF FIGURES

CHAPTER 1

INTRODUCTION

Quite often we encounter fluid flow and heat transfer in cavities at different orientations. These classical problems have some analytical and huge numerical solutions. Heat line analysis for mixed convection flow in cavities and channels have been studied by many researchers and it has been a very popular research topic for many years. Heatline analysis for mixed convection flows are important in the context of many engineering applications for predicting the performance, designing of many equipment, machine parts like microchips to large nuclear reactor. But things used in practical purpose are much more complicated in design and prediction of their performance using results from simple geometry cause huge error. For this complexity, in recent years, attention has been given to study thermal characteristics of complex geometry. Among those the cavities with solid bodies or partitions are given special attention due to their wide applications in heat exchangers, solar heat collector, some air conditioning equipment etc.

A study of the flow of nanofluid in a cavity with heat generating obstacles is also important from the technical point of view and such type of problems have received much attention by many investigators. Mathematical models used to predict the flow and the thermal behavior are mainly a couple of non-linear partial differential equations and their analytic solution is impossible except some special cases.

The rest of the introductory chapter is as follows: since the problems that we shall study in this thesis are heat line analysis and mixed convection flow in cavities, we begin with a brief description on types of heat transfer in section 1.1 and mixed convection heat transfer in cavities in section 1.2. Then reviews on some definitions has been given in section 1.3. For convenience of present investigation literature related to this study has been presented briefly in section 1.4, then the motivation behind selection of the present problem, description and objective of the current study are described in section 1.5 to

1.7. Finally in section 1.8, a brief outline of the remainder of the thesis has been presented.

1.1 Types of Heat Transfer

Heat transfer is the process of transportation of thermal energy from one region to another region due to temperature difference. The heat transfer takes place by the distinct mechanisms or modes: Conduction, Convection and Radiation. The heat transfer always takes place from higher temperature medium to lower temperature one and heat transfer stops when the two mediums reaches the same temperature.

Conduction is the transfer of energy from the higher energetic particle of a substance to adjacent lower energetic one as a result of interactions between the particles. Conduction can take place in solids, liquids, or gases. In gases and liquids, conduction is due to the collisions and diffusion of the molecules during their random motion, in solids it is due to the combination of vibrations of the molecules in a lattice and the energy transport by free electrons. The rate of heat conduction through a medium depends on the geometry of the medium, its thickness and the material of the medium, as well as the temperature difference across the medium.

Convection is the mechanism of heat transfer through a fluid in the presence of bulk fluid motion resulting from the temperature difference. This type of heat transfer is called convection. The convection of heat transfer is of two types: natural convection and forced convection. If the fluid flow via convection occurs naturally, the convection is called natural (or free) convection. In this case fluid motion is set up by buoyancy effects resulting from the density variation caused by the temperature difference in the fluid and gravitational force. On the other hand, if the fluid motion is artificially created by means of external source like a blower or fan, the heat transfer mode is called forced convection.

Radiation is the energy emitted by matter in the form of electromagnetic waves (or photons) as a result of the changes in the electronic configuration of the atom or molecules. Unlike conduction and convection, the transfer of heat by radiation does not require the presence of an intervening medium. In fact, heat transfer by radiation is faster

and suffers no attenuation in a vacuum. This is how the energy of the sun reaches the earth. Radiation is a volumetric phenomenon, and all solids, liquids, and gases emit, absorb, or transmit radiation to varying degrees. However, radiation is usually considered to be a surface phenomenon for solids that are opaque to thermal radiation such as metals, wood and rocks.

1.2 Mixed Convection Heat Transfer in Cavities

Mixed convection occurs when natural and forced convection mechanism acts together. Mixed convection in cavities is a contemporary importance, because cavities filled with fluid are central components in a long list of engineering and geophysical systems. The flow and the heat transfer induced in a cavity differs fundamentally from the external mixed convection boundary layers. Mixed convection in a cavity is the result of the complex interaction between finite size fluid systems in thermal communication with all the walls that confine it. The complexity of this internal reaction is responsible for the diversity of flow. Based on the potential engineering application, the cavity phenomena can be classified into two classes:

a. Vented cavity and
b. Lid driven cavity

In a vented cavity flows induced by the heat source leads to the possibility of complex flows. The fluid flow and the heat transfer in a lid driven cavity where the flows are induced by a shear force resulting from the motion of a lid combined with the buoyancy force due to the non-homogeneous temperature of the cavity wall. The interaction between the buoyancy driven and shear driven flows inside a closed cavity in a mixed convection regime is quite complex. That is why it is important to understand the fluid flow and heat transfer characteristics of mixed convection in a lid driven cavity.

1.3 Some Definitions

Viscosity

The viscosity of a fluid which is a strong function of temperature is a measure of its resistance to deformation. A friction force develops between two adjacent fluid layers

while they move relative to each other and the slower layer tries to slow down the faster layer. This type of internal resistance to flow is quantified by the fluid property viscosity. All fluid flows involve viscous effects to some degree and therefore no fluid are of zero viscosity. As temperature increases, the viscosity of liquids decreases whereas the viscosity of gases increases with temperature.

Viscous and non- viscous flow

Flows are called viscous whose flow patterns are dominated by the viscous properties of the fluid. This arises in fluids where the velocity gradients are comparatively large. The flow close to the walls of the pipes can be treated as viscous flows.

The flow is defined as non-viscous or inviscid flow if the viscous properties are not dominant. These types of flows are common in the center region of flow in pipes and in gas flows.

Newtonian and non-Newtonian fluid

Newtonian fluids are those fluids for which the constant of proportionality i.e. the co-efficient of viscosity (μ) does not change with the rate of deformation. In other words, fluids that follow the Newton's law of viscosity are known as Newtonian fluids. Water, air and mercury are some examples of Newtonian fluids.

Non-Newtonian fluids are those fluids for which the constant of proportionality i.e. the co-efficient of viscosity (μ) changes with the rate of deformation. In other words, fluids that do not follow the Newton's law of viscosity are known as non-Newtonian fluids. Blood, liquid plastic and polymer solutions are non-Newtonian fluids.

Compressibility

Compressibility is a property of fluid that measures the change in density and consequently, the change in the volume of a fluid during motion under the action of external forces. The compressibility is expressed in terms of Mach number (M) which is defined by $M = \dfrac{\text{speed of fluid}}{\text{speed of sound}} = \dfrac{u}{\alpha_0}$.

Compressible and incompressible flow

A compressible flow is one in which the density varies in the different portion of the fluids. Thus the volume of every portion of fluid differs in compressible flow over the course of its motion. A flow is said to be incompressible if the density remains nearly constant throughout. Therefore, for incompressible flow the volume of every portion of fluid remains unchanged over the course of its motion. The density of liquids is basically constant and accordingly the flow of liquids is naturally referred to as incompressible.

Internal and external flow

A fluid flow is classified into two categories; internal and external, depending on whether the fluid is forced to flow in a confined channel or over a surface. An internal flow is in a channel bounded on all sides by a solid surface except, possibly, for an inlet and exit. Flows through a pipe or in an air-conditioning duct are the examples of internal flow. Internal flows are dominated by the influence of viscosity throughout the flow field. The flow of an unbounded fluid over a surface is external flow.

Thermal diffusivity

Thermal diffusivity represents how fast heat diffuses through a material and is defined as $\alpha =$ Heat conducted /Heat stored$= \dfrac{k}{\rho c_p}$.

Here the thermal conductivity k represents how well a material conducts heat and the heat capacity ρc_p represents how much energy a material stores per unit volume. Therefore, the thermal diffusivity of material can be viewed as the ratio of the heat conducted through the material to the heat stored per unit volume. A material that has a high thermal conductivity or a low heat capacity will obviously have a large thermal diffusivity. The large thermal diffusivity means that the propagation of heat into the medium is faster. A small value of thermal diffusivity means the heat is mostly absorbed by the material and a small amount of heat is conducted further.

Thermal conductivity

Thermal conductivity is defined as the quantity of heat (Q) transmitted through a unit thickness (L) in a direction normal to a surface of unit area (A) due to a unit temperature gradient (ΔT) under steady state conditions and when the heat transfer is dependent only on the temperature gradient. In equation form this becomes the following:

Thermal Conductivity = heat × distance / (area × temperature gradient)

$$k = Q \times L / (A \times \Delta T)$$

Heatlines

Heatlines represent heat flux lines which represents the trajectory of the heat flow and they are normal to the isotherms for conductive heat transfer. Heat functions are mathematical representation of heatlines and each heatline contour corresponds to constant heat functions. Heatline is the best tool to analyze and understand the heat flow in 2D convective transport process and this concept is similar to streamline which is important to analyze the heat motion.

Nanofluids

A nanofluid is a fluid containing nanometer sized particles called nanoparticles. These fluids are engineered colloidal suspensions of nanoparticles in a base fluid. The nanoparticles used in nanofluids are typically made of metals, carbides or carbon nanotubes. Nanofluids are two phase systems with one phase (solid phase) in another (liquid phase). Nanofluids have been found to process enhanced thermo physical properties such as thermal conductivity, thermal diffusivity, viscosity and connective heat transfer co-efficient compared to those of base fluids like oil or water. For a two phase system, one of the most important issue is the stability of the nanofluid and it is a big challenge to achieve desired stability of nanofluids. The potentials of nanofluids in heat transfer have attracted more and more attention. Due to high density of chips, design of electronic components with more compact makes heat dissipation more difficult. Recent Researchers illustrated that nanofluids could increase the heat transfer coefficient by increasing the thermal conductivity of a coolant.

1.3.1. Dimensionless parameters

The dimensionless parameters can be considered as measures of the relative importance of certain aspects of the flow. Some dimensionless parameters related to the present study are discussed below:

(a) Prandtl number

The relative thickness of the velocity and the thermal boundary layers are best described by the dimensionless parameter Prandtl number, defined as

$$Pr = \frac{v}{\alpha} = \frac{\text{Viscous diffusion rate}}{\text{Thermal diffusion rate}} = \frac{c_p \mu}{k}$$

Where $v = \dfrac{\mu}{\rho}$ is the kinematic viscosity, $\alpha = \dfrac{k}{(\rho c_p)}$ is the thermal diffusivity, μ is the dynamic viscosity, k is the thermal conductivity, c_p is the specific heat and ρ is the density. It is named after Ludwing Prandtl, who introduced the concept of boundary layer in 1904 and made significant contributions to boundary layer theory. The Prandtl number of fluids ranges from less than 0.01 for liquid metals to more than 100,000 for heavy oils.

(b) Reynolds number

The transition from laminar to turbulent flow depends on the surface geometry, surface roughness, flow velocity, surface temperature and type of fluid, among other things. In 1883 Osborn Reynolds discovered that the flow regime depends mainly on the ratio of the inertia forces to friction forces in the fluid. This ratio is called the Reynolds number, which is a dimensionless quantity, and is defined as

$$Re = \frac{inertia\ Force}{Friction\ Force} = \frac{Mass \times Accelaretion}{Shering\ Stress \times Cross\ sec\ tional\ Area}$$

$$= \frac{Volume \times Density \times (Velocity\ /\ Time)}{\mu \times (Velocity\ /\ Length) \times Cross\ Sectional\ Area}$$

$$= \frac{(Length)^3 \times Density \times (Length\ /\ Time)}{\mu \times (Length)^2}$$

$$= \frac{Length \times Density \times Velosity}{\mu} = \frac{L \times \rho \times V}{\mu} = \frac{LV}{\mu\ /\ \rho} = \frac{LV}{\nu}$$

Here V, L, ρ and μ. are characteristic values of reference velocity, characteristic length, density and coefficient of viscosity of the fluid flow respectively and $\nu = \dfrac{\mu}{\rho}$ is the kinematic viscosity.

(c) Rayleigh number

The Rayleigh number for a fluid is a dimensionless number associated with the heat transfer within the fluid. When the Rayleigh number is below the critical value for that fluid, heat transfer is primary in the form of conduction; when it exceeds the critical value, heat transfer is primarily in the form of convection. The Rayleigh number is named after Lord Rayleigh and is defined as the product of the Grashof number, which describes the relationship between buoyancy and viscosity within a fluid, and the Prandtl number, which describes the relationship between momentum diffusivity and thermal diffusivity.

For free convection near a vertical wall, this number is

$$Ra_x = Gr_x \Pr = \frac{g\beta}{\nu\alpha}\left(T_s - T_\infty\right)x^3$$

where

Pr = Prandtl number

g = gravity

x = characteristic length (in this case, length of cavity)

T_s = temperature of surface

T_∞ = quiescent temperature

v = kinematic viscosity

α = thermal diffusivity

β = thermal expansion coefficient

Fluid properties Pr, v, α and β are evaluated at the field temperature, which is defined

as $T_f = \dfrac{T_s + T_\infty}{2}$

For most engineering purposes, the Rayleigh number is large, somewhere around 10^6 and 10^8.

1.4 Literature Review

Mixed convection is the combination of free and forced convective flow in which neither the free convection nor the forced convection effects are dominant. The effect of mixed convective flows in cavities, channels are investigated by many researchers by using analytical, numerical and experimental methods. Such a problem is grouped under lid driven cavity problem. The modeling and simulations of crystal growth, glass production, nuclear reactors and food processing are common examples of current industrial applications while convective thermal currents associated with the flow structure occurring in the lakes and reservoirs are classically sited as natural phenomenon.

Heat transfers are needed in modern technology and are very important in many industrial areas. Hence it is necessary to study and simulate heat transfer phenomena. In recent years heat transfer in cavities in present of obstacles has drawn special attention and many authors have recently studied heat transfer in cavities with obstacles like heat generating objects, partitions and fins to the wall(s).

Some important works are presented below:

Aydin and Yang [2] numerically studied the transport mechanism of laminar mixed convective in a shear and buoyancy-driven cavity. Mixed convective heat transfer in a two dimensional rectangular cavity with constant heat flux from partially heated bottom wall while the isothermal sidewalls are moving in a vertical direction was numerically studied by Gau and Sharif [21]. Luo and Yang [26] investigated two dimensional flow in a two-sided lid-driven cavity containing a temperature gradient. Billah et al. [6] investigated heat transfer and flow characteristics for MHD mixed convection in a lid driven cavity with heat generating obstacles where the horizontal walls of the cavity were kept adiabatic.

Aminossadati and Ghasemi [1] performed a numerical study on the mixed convection in a horizontal channel with a discrete heat source in an open cavity. They considered three different heating modes and found noticeable differences among the indicated three heating modes. Mixed convection heat transfer in open-ended enclosures has been studied numerically for three different flow angles of attack by Khanafer et al. [23]. Leong et al. [25] performed a numerical study on the mixed convection from an open cavity in a horizontal channel. Authors found that the heat transfer rate was reduced, and the flow became unstable in the mixed convection regime. A numerical analysis of laminar mixed convection in a channel with an open cavity and a heated wall bounded by a horizontally insulted plate was presented in Manca et al. [29], where they considered three heating modes: assisting flow, opposing flow and heating from below. Later on, similar problem for the case of assisting forced flow configuration was tested experimentally by Manca et al. [28]. Steady laminar mixed convection inside a lid-driven square cavity filled with water is studied numerically by Chamkha et al. [9]. They have shown the results that there are critical values for the partial slip parameter at which the convection is declined.

Rahman et al. [41] performed the effect of Reynolds and Prandtl numbers on mixed convection in an obstructed vented cavity. They found that the flow and thermal field strongly depend on the Reynolds number, Prandtl number as well as Richardson number. As the Reynolds number and Prandtl number increase, the heat transfer rate

increases but average fluid temperature in the cavity and temperature at the cylinder center decrease at the three convective regimes. Then after Rahman et al. [42] investigated mixed convection inside a square ventilated cavity with a heat generating solid body located at the center. It was observed that heat transfer had a strong relation with conductivity ratio between solid and fluid as well as the diameter of the heat generating body. They found that the flow and temperature field is strongly dependent on the parameters D, K, and Q for the ranges considered. Yapici et al. [47] investigated laminar mixed convection in a lid-driven square cavity considering different shapes of hot bottom wall. It was found that at low Ri, rectangular wave shaped bottom wall produced maximum heat transfer. Numerical analysis on mixed convection heat transfer of nanofluid in a channel is investigated by Rashidi et al. [43]. Numerical simulation of mixed convection within nanofluid filled cavities was studied by Esfe et al. [19]. Muhtamilselvan et al. [32] have used copper-water nanofluids for the heat transfer enhancement.

Parvin et al. [37] also investigated the effect of Reynolds number for mixed convection flow of nanofluid in a double lid driven cavity with heat generating obstacle. The study of two-dimensional mixed convection from a heated square solid cylinder located at the center of a vented cavity filled with air (Pr = 0.71) is performed.by Chamkha et al. [8].The results show that the average Nusselt number along the heated surface of the inner square values increases with increasing values of the Reynolds and Richardson numbers. The effect of the locations of the inner square cylinder and aspect ratio is found to play a significant role in the streamline and isotherm patterns. A channel with a cavity heated from below is numerically investigated for the mixed convection case for a range of Richardson numbers (Ri = 0.1, 1, 5, 10, 15 and 20) and Reynolds numbers (Re = 400, 500, 600, 700 and 800) in the laminar flow regime is investigated by Fatih [20]. Mixed convection flows in a lid-driven square cavity filled with porous medium are studied numerically using penalty finite element analysis for uniformly heated bottom wall, linearly heated side walls or cooled right wall by Basak et al. [3]. They found that the isotherms are generally symmetric at smaller Pr irrespective of Da and Re at $Gr = 10^5$ for linearly heated side walls. The isotherms are also almost symmetric at small Re with higher Gr ($Gr = 10^5$) and Da ($Da = 10^{-3}$) and natural convection is found

to be dominant whereas the isotherms are compressed near the left and bottom walls at higher Re for linearly heated side walls.

Melting heat transfer influence on nanofluid flow inside a cavity in existence of magnetic field is studied by Sheikholeslami and Rokni [45]. KKL model is taken into account to obtain viscosity and thermal conductivity of CuO-water nanofluid. Roles of melting parameter (δ), CuO-water volume fraction (χ), Hartmann (Ha) and Rayleigh (Ra) numbers are illustrated in outputs. Results depict that temperature gradient enhances with rise of Rayleigh and melting parameter. Nusselt number decreases with increase of Lorentz forces.

A combined free and forced convection flow of an electrically conducting fluid in a cavity or in a channel in the presence of magnetic field is of special technical significance because of its frequent occurrence in many industrial applications such as geothermal reservoirs, cooling of nuclear reactors, thermal insulations and petroleum reservoirs. A study of magnetohydrodynamic (MHD) mixed convection around a heat conducting horizontal circular cylinder placed at the center of a rectangular cavity along with joule heating has been carried out by Rahman et al. [40]. It was found that the streamlines, isotherms, average Nusselt number, average fluid temperature and dimensionless temperature at the cylinder center strongly depend on the Richardson number, Hartmann number and the cavity aspect ratio. After a few years a finite element analysis is performed by Rahman et al. [38] on the conjugated effect of joule heating and magnetohydrodynamic on double-diffusive mixed convection in a horizontal channel with an open cavity. The results represented that the parameters like as Richardson number, Hartmann number, joule heating, buoyancy ratio and Lewis number have noticeable effect on the flow pattern and heat and mass transfer. On the same time, the development of magnetic field effect on mixed convective flow in a horizontal channel with a bottom heated open enclosure has been numerically studied again by Rahman et al. [39]. The results indicate that the parameters like as Rayleigh number, Reynolds number and Hartmann number strongly affect the flow phenomenon and temperature field inside the cavity whereas in the channel these effects are less significant.

Heat transfer has been given an enormous importance now a day as many engineering and modern science and technology system involves the problem of heat transfer. In most of the case it has been observed that traditional fluid cannot meet the demand of the desired thermo physical property which is needed for the desired level of heat transfer. As a result scientists and researcher are now a day trying different fluid to increase the heat transfer rate. The thermal conductivities of several nanofluids (dispersions of alumina nanoparticles in ethylene glycol) were measured at temperatures ranging from 298 to 411 K using a liquid metal transient hot wire apparatus is investigated by Beck et al. [4]. Their results confirm that additional temperature contributions inherent in Brownian motion models are not necessary to describe the temperature dependence of the thermal conductivity of nanofluids. Experimental investigations and theoretical determination of effective thermal conductivity and viscosity of Al_2O_3/H_2O nanofluids are reported by Chandrasekar et al. [10]. The thermal conductivity and viscosity of nanofluids are measured and it is found that the viscosity increase is substantially higher than the increase in thermal conductivity. Both the thermal conductivity and viscosity of nanofluids increase with the nanoparticle volume concentration. Also they found that the proposed models show reasonably good agreement with their experimental results. Experiments are carried out by Chen et al. [11] on the rheological behavior of ethylene glycol (EG) based titanate nanotubes (TNT) nanofluids containing 0.5, 1.0, 2.0, 4.0 and 8.0 wt. % TNT at 20–60 °C. Their results show a very strong shear thinning behavior of the TNT nanofluids and big influences of particle concentration and temperature on the zero shear viscosity (ZSV) and high shear viscosity (HSV), for which the conventional form of Brenner & Condiff equation fails to predict. Choi [12] investigated Nanofluids: From vision to reality through research. He highlights recent advances in this new field of research and shows future directions in nanofluids research through which the vision of nanofluids can be turned into reality.

A numerical investigation of mixed convection due to a copper–water nanofluid in a Lid –Driven square enclosure is presented by Nayak et al. [34]. They obtained the enhancement rate in heat transfer and entropy generation in nanofluid for a wide range of parameter values. The experimental results from a study on diathermic oil based nanofluids are executed by Colangelo et al. [13]. The results showed that the heat

transfer performance of diathermic oil enhances more than water with the same nanoparticles. Two empirical correlations for predicting the effective thermal conductivity and dynamic viscosity of nanofluids, based on a high number of experimental data available in the literature, are proposed and discussed by Corcione [14]. They found that, given the nanoparticle material and the base fluid, the ratio between the thermal conductivities of the nanofluid and the pure base liquid increases as the nanoparticle volume fraction and the temperature are increased, and the nanoparticle diameter is decreased. Additionally, also the ratio between the dynamic viscosities of the nanofluid and the pure base liquid increases as the nanoparticle volume fraction is increased, and the nanoparticle diameter is decreased, being practically independent of temperature. The heat transfer features of buoyancy-driven nanofluids inside rectangular enclosures differentially heated at the vertical walls are investigated theoretically by Corcione [15]. They observed that for any assigned combination of solid and liquid phases, the optimal volume fraction is found to increase slightly with decreasing the nanoparticle size, and to increase much more remarkably with increasing both the nanofluid average temperature and the slenderness of the enclosure. The numerical modeling of steady laminar mixed convection flow in a lid-driven cavity with a wavy wall filled with a water–CuO nanofluid is focused by Nada and Chamkha [33]. They found that the presence of nanoparticles causes significant heat transfer augmentation for all values of Richardson numbers and bottom wall geometry ratios. A numerical study is carried out by Hasib et al. [22] to investigate the transition from laminar to chaos in mixed convection heat transfer inside a lid-driven trapezoidal enclosure. It is found that both the flow and the temperature profiles are influenced by the combined effect of Reynolds and Grashof numbers to a great extent.

The heatline concept was first introduced by Kimura and Bejan [24]. Various applications using heatlines were studied by Bello-Ochende [5], Costa [16], Mukhopadhyay et al. [31] and Deng and Tang [18]. Dalal and Das [17] have used heat line method for the visualization of flow in a complicated cavity. However a comprehensive analysis on heat flow during the mixed convection in a lid driven cavity with the heatline approach is yet to appear in this literature.

Heat flow visualization during mixed convection within entrapped porous triangular cavities with moving horizontal walls via heatline analysis was studied by Roy et al. [44]. There they have considered two cases, case 1: hot horizontal walls and cold inclined walls; case 2: cold horizontal walls and hot inclined walls. Again heatline analysis for MHD mixed convection flow of nanofluid in a driven cavity with heat generating block was studied by Parvin and Siddiqua [36]. Heat transfer enhancement by nanofluid in a cavity containing a heated obstacle is analyzed by Parvin et al. [35]. Again heatlines and other different visualization methods for confined heat transfer system are discussed by Mahapatra et al. [27]. For convective heat transfer problems, most widely used techniques to visualize the fluid flow and heat transfer are streamlines and isotherms respectively. These methods are not sufficient to address the degrees of complexity associated with the complicated convective problems. Thus, different visualization techniques have been developed to represent the results depending on the problem. Again the article by Sheikholeslami et al. [46] explores the effect of thermal radiation on Al_2O_3-water nanofluid flow and heat transfer in an enclosure with a constant flux heating element. The effects of Rayleigh number, Hartman number, viscous dissipation parameter, radiation parameter, volume fraction of nanoparticle on the flow and heat transfer characteristics have been examined.

1.5 Applications

Mixed convection heat transfer has always been of great interest because of its wide applications in different engineering areas such as the cooling systems of electronic components, building and thermal insulation systems, the built-in-storage solar collectors, the nuclear reactor systems, the food storage industry and the geophysical fluid mechanics and chemical processing equipment. Moreover mixed convection heat transfer enhancement of nanofluids are expansively used in various sizes of electrical and electronic devices. Also nanofluids are now being developed for medical applications, including cancer therapy and safer surgery by cooling. However, Nanofluids technology can help to develop better oils and lubricants.

1.6 Motivation behind Selection of the Present Problem

It is clear from the literature review that little numerical study on heat line analysis for mixed convection flow of nanofluids in a cavity with heat generating block has been carried out. Heat line analysis for mixed convection in a cavity is important for numerous engineering applications. Mixed convection heat transfer is very important in designing nuclear reactor, solar collectors, electrical, micro electrical equipment containers and in many other design problems. Thus the analysis of the effect of mixed convection for different boundary conditions and shapes are necessary to ensure efficient performance of heat transfer equipment. On the other hand, the majority of the mixed convection studies were carried out in channel or cavity. Numerous studies on nanofluids are being conducted by talented thermal scientists and engineers all over the world, and they have made the scientific breakthrough not only in discovering unexpected thermal properties of nanofluids, but also in proposing new mechanisms behind the enhanced thermal properties of nanofluids and thus identifying unusual opportunities to develop them as next generation coolants for computers and safe coolants for nuclear reactors. Researchers have started showing interest in the study of heat transfer characteristics of these nanofluids in recent years.   If the cavity contains nanofluids and heat generating object is placed inside the cavity then the rate of heat transfer draws an extra attention. To the best of my knowledge, a little attention has been paid to investigate the heat transfer characteristics of the nanofluids contained in a cavity containing heat generating object. Numerical studies are therefore essential to observe the variation in fluid flow and heat transfer due to the above physical and properties changes, which forms the basis for the motivation behind the present study.

1.7 Present Problem

In the above studies it is observed that, the heatline analysis for mixed convection in a square with cavity with heat generating object using nanofluids has not been analyzed yet. The study will be carried out numerically with an accurate numerical procedure, and the related results will be shown using isotherms, streamlines, heatlines, and related graphs and charts. The challenge of augmentation of heat transfer can be met with this model.

The specific objectives of the present research work are:

- To study a mathematical model regarding the mixed convection flow around a heat generating block placed in a double lid-driven cavity filled with nanofluid.

- To solve the mathematical model using Finite Element Method (**FEM)**.

- To examine the effect of different parameters namely Reynold's number Re, solid fluid thermal conductivity ratio (K), Richardson's number Ri, heat generation parameter (Q) and solid volume fraction (χ), on isotherms, streamlines, heatlines and average heat transfer.

- To make an optimum combination of the aforesaid parameters.

- To validate the present computational procedure with other published works.

It is expected that the present numerical investigation will contribute to the search for finding more efficient and better renewable energy equipment.

1.8 Outline of the Thesis

This thesis paper contains four chapters. In chapter 1, a brief introduction is presented with aim and objective. This chapter also consists a literature review of the past studies on fluid flow and heat transfer in cavities or channels. In this state-of-the art review, different aspects of the previous studies have been mentioned categorically. This is

followed by the post-mortem of a recent historical event for the illustration of fluid flow and heat transfer effects in cavities or channels.

In Chapter 2, the computational procedure of the problem for viscuss incompressible flow of nanofluid. Basically finite element method is employed in this study and explained elaborately. We have investigated the effects for mixed convection flow in a lid driven cavity with water-alumina nanofluids.

Chapter 3 contains a detailed parametric study on heatline analysis of mixed convection flow of nanofluid in a cavity with heat generating object. Effects of the major parameters such as Reynolds number, solid fluid thermal conductivity ratio, Richardson's number, heat generation parameter, solid volume fraction, on the isotherms, streamlines and heatline are described.

Finally, in Chapter 4 the dissertation is rounded off with the conclusions. Lastly, recommendations for further study of the present problem are outlined.

CHAPTER 2

PHYSICAL MODEL AND COMPUTATIONAL DETAILS

The mathematical model of physical phenomena may be ordinary or partial differential equations, which have been the subject of numerical and analytical investigations. The governing partial differential equations of fluid mechanics and heat transfer are solvable for only a limited number of flows. To determine an approximate solution numerically, we have to use a discretization method which approximated the differential equations by a system of algebraic equations, which can then be solved on a computer. The approximations are used to small domains in space and /or time so the numerical solution provides results at discrete locations in space and time. Much as the accuracy of experimental data depends on the quality of the tools used, the accuracy of numerical solutions is dependent on the quality of discretization used.

Computational fluid dynamics (CFD) computation involves the formation of a set numbers that constitutes a practical approximation of a real life system. The outcome of computation process improves the understanding of the performance of a system. Thereby, engineers need CFD codes that can make physically realistic results with good quality accuracy in simulations with finite grids. Contained within the broad field of computational fluid dynamics are activities that cover the range from the automation of well-established engineering design methods to the use of detailed solutions of the Navier-Stokes equations as substitutes for experimental research into the nature of complex flows. CFD have been used for solving wide range of fluid dynamics problem. It is more frequently used in fields of engineering where the geometry is complicated or some important feature that cannot be dealt with standard methods.

The analysis of flow and heat transfer in thermodynamics can be performed either theoretically or experimentally. Experimental study of such problem could not gain that much popularity in the field of thermodynamics because of their limited flexibility and applications. For every change of geometry and boundary conditions, it needs separate

investigation, involving separate experimental requirement/ arrangement, which, in turn makes it unattractive, especially, from the time involved and economical point of views.

The remainder of this chapter is as follows. In section 2.1, the physical configurations of the current research interest are shown. Then the appropriate mathematical model (both governing equations and boundary conditions) is considered in section 2.2. After that a numerical scheme that is employed in this study are described in the section 2.3.

2.1 Physical Configurations
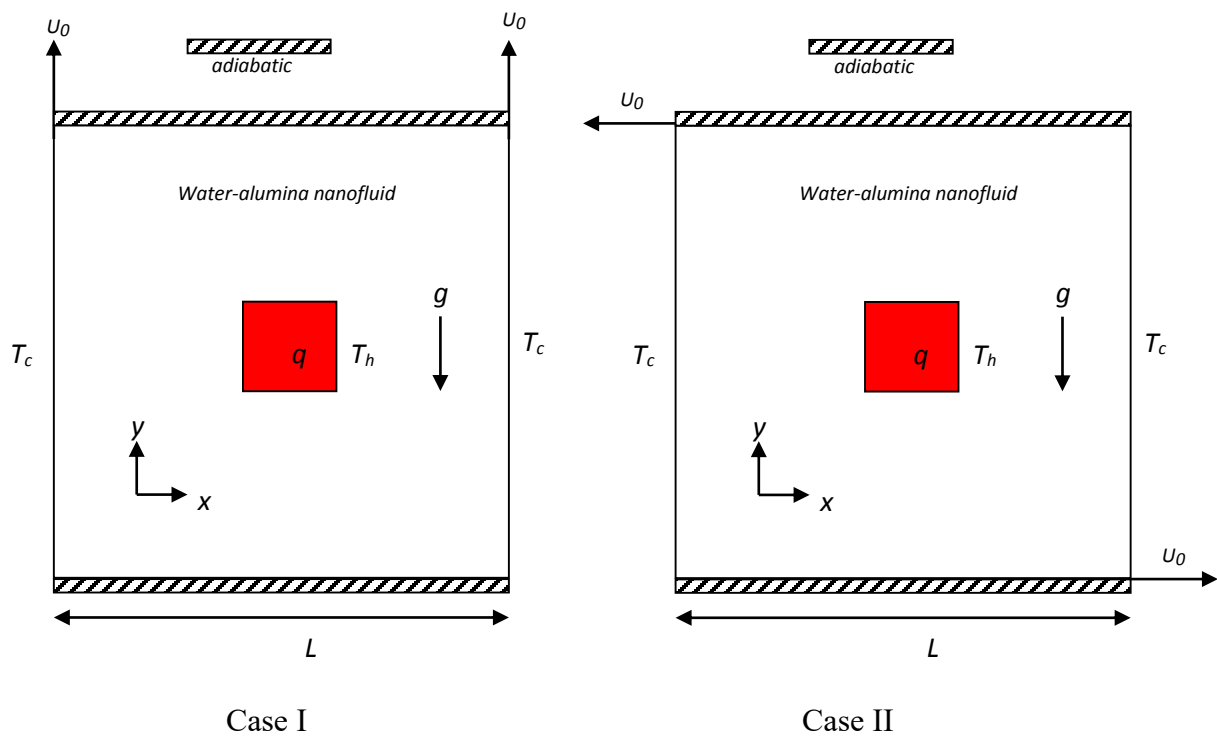
Figure 2.1: Schematic diagram of the problem

The schematic of the problem herein investigated is presented in the figure 2.1. A Cartesian co-ordinate system is used with the origin at the lower left corner of the computational domain. The system consists of a double-lid-driven square enclosure with sides of length L. A heat generating solid square obstacle is positioned at the center of the cavity. In

addition, the cavity is saturated with electrically conducting water alumina nanofluid. The solid obstacle has a thermal conductivity of k_s and generates uniform heat flux (q) per unit area. Moreover, the vertical walls of the cavity are mechanically lid-driven and considered to be at a constant temperature T_c and both the top and bottom surfaces of the enclosure are kept adiabatic. Furthermore, the vertical walls are at uniform velocity U_0 in the positive y direction (upward) (case I), the top wall is moving left and bottom wall is moving right with the same velocity U_0 (case II).

2.2 Mathematical Formulation

In order to solve the fluid flow problems, some fundamental laws are used such as the law of conservation of mass or continuity equation, conservation of momentum, and conservation of energy, which constitute a set of coupled, nonlinear, partial differential equations. The nanofluids in the enclosure are Newtonian, incompressible and laminar. The nanoparticles are assumed to have uniform shape and size. It is considered that thermal equilibrium exists between water and nanoparticles (Al_2O_3 nanoparticles) and no slip occurs between the two media. It should be stated that, in a practical situation, most nanofluids used for augmentation of heat transfer are made up of extremely fine particles, usually under 40 nm diameter. The thermo-physical properties of water-alumina nanofluids are listed in Table 2.1.

Table 2.1. Thermophysical properties of water and alumina Mansour [30]

Property	Fluid phase (water)	Solid phase (alumina)
c_p (J Kg^{-1} K^{-1})	4179	765
ρ (Kg m^{-3})	997.1	3970
k (W m^{-1} K^{-1})	0.613	40
β (K^{-1})	2.1×10^{-4}	0.85×10^{-5}

The several steps of the mathematical formulations for the above physical configurations are shown as follows:

2.2.1 Governing equations

The physical properties of the nanofluids are considered to be constant except the density variation in the body force term of the momentum equation which is satisfied by the Boussinesq's approximation. The effects of radiation and viscous dissipation are neglected. Under the above assumptions, the system of equations governing the two-dimensional motion of nanofluids is as follows:

Continuity Equation

$$\frac{\partial u}{\partial x} + \frac{\partial v}{\partial y} = 0 \tag{2.1}$$

Momentum Equations

$$u\frac{\partial u}{\partial x} + v\frac{\partial u}{\partial y} = -\frac{1}{\rho_{nf}}\frac{\partial p}{\partial x} + \nu_{nf}\nabla^2 u \tag{2.2}$$

$$u\frac{\partial v}{\partial x} + v\frac{\partial v}{\partial y} = -\frac{1}{\rho_{nf}}\frac{\partial p}{\partial y} + \nu_{nf}\nabla^2 v + \frac{(\rho\beta)_{nf}}{\rho_{nf}}g(T - T_c) \tag{2.3}$$

Energy Equations

$$u\frac{\partial T}{\partial x} + v\frac{\partial T}{\partial y} = \alpha_{nf}\nabla^2 T \tag{2.4}$$

For solid obstacle the energy equation is, $\nabla^2 T_s + q = 0$ \hfill (2.5)

where x and y are the distances measured along the horizontal and vertical directions respectively, u and v are the velocity components in the x and y directions respectively, T and T_s denotes the fluid and solid temperature respectively, T_c denotes the reference temperature for which buoyancy force vanishes, p is the pressure and ρ is the density of the fluid, g is the gravitational constant, β is the volumetric coefficient of thermal expansion, c_p is the fluid specific heat, k and k_s are the thermal conductivity of the fluid and solid respectively.

The effective density ρ_{nf} of a fluid containing suspended particles at a reference temperature is given by

$$\rho_{nf} = \chi\,\rho_p + (1 - \chi)\rho_f \tag{2.6}$$

where χ is the solid volume fraction of nanoparticles. In addition, the thermal diffusivity α_{nf} of the nanofluids can be expressed as:

$$\alpha_{nf} = \frac{k_{nf}}{(\rho c_p)_{nf}} \tag{2.7}$$

The heat capacitance of nanofluids can be defined as

$$(\rho c_p)_{nf} = \chi(\rho c_p)_p + (1 - \chi)(\rho c_p)_f \tag{2.8}$$

Additionally, the thermal expansion coefficient of the nanofluids $(\rho\beta)_{nf}$ is expressed as:

$$(\rho\beta)_{nf} = \chi(\rho\beta)_p + (1 - \chi)(\rho\beta)_f \tag{2.9}$$

The viscosity of the nanofluids can be estimated with the existing relations for the two-phase mixture.

The equation given by Brinkman [7] has been used as the relation for dynamic viscosity of the nanofluids in this problem, as given

$$\mu_{nf} = \frac{\mu_f}{(1-\chi)^{2.5}} \tag{2.10}$$

The effective thermal conductivity of nanofluids, k_{nf}, is given by

$$\frac{k_{nf}}{k_f} = \frac{k_p + 2k_f - 2\chi(k_f - k_p)}{k_p + 2k_f + 2\chi(k_f - k_p)} \tag{2.11}$$

where, k_p is the thermal conductivity of the nanoparticles and k_f is the thermal conductivity of base fluid and χ is the particle volume fraction of the suspension.

2.2.2 Boundary conditions (dimensional form)

For the present problem the boundary conditions are specified as follows:

For case I:

At sliding double leads: $u = 0, v = U_0, T = T_c$

At horizontal top and bottom walls: $u = v = 0, \dfrac{\partial T}{\partial n} = 0$

At square block boundaries: $u = v = 0, T = T_h$

At fluid solid interface: $\left(\dfrac{\partial T}{\partial n}\right)_{\text{fluid}} = k \left(\dfrac{\partial T_s}{\partial n}\right)_{\text{solid}}$

For case II:

At horizontal top wall: $u = -U_0, v = 0, \dfrac{\partial T}{\partial n} = 0$

At horizontal bottom wall: $u = U_0, v = 0, \dfrac{\partial T}{\partial n} = 0$

At the vertical walls: $u = v = 0, T = T_c$

At square block boundaries: $u = v = 0, T = T_h$

At fluid solid interface: $\left(\dfrac{\partial T}{\partial n}\right)_{\text{fluid}} = k \left(\dfrac{\partial T_s}{\partial n}\right)_{\text{solid}}$

Where n is the non-dimensional distances either in x or y direction acting normal to the surface and k is the ratio of the solid fluid thermal conductivity k_s/k_{nf}.

Such local values have been further averaged over the entire heated surface to obtain the surface averaged or overall mean Nusselt number

$$Nu_{av} = -\frac{1}{L}\int_0^L \frac{\partial T}{\partial N}ds$$

where L is the length of the heated wall. The average Nusselt number can be used in process engineering design calculations to estimate the rate transfer from the heated surface.

2.2.3 Dimensional analysis

The following dimensionless parameters are introduced for making the governing equations (2.1−2.5) into dimensionless form:

$$X = \frac{x}{L}, \ \ Y = \frac{y}{L}, V = \frac{v}{U_0}, U = \frac{u}{U_0}, \Delta T = T_h - T_c, \theta = \frac{T-T_c}{\Delta T}, P = \frac{p}{\rho_{nf} U_0^2}$$

where X and Y are the coordinates varying along horizontal and vertical directions, respectively, U and V are, the velocity components in the X and Y directions, respectively, θ is the dimensionless temperature and P is the dimensionless pressure. After substitution the dimensionless variables into the equations (2.1-2.5), we get the following dimensionless equations as

Continuity equation

$$\frac{\partial U}{\partial X} + \frac{\partial V}{\partial Y} = 0 \tag{2.12}$$

Momentum equations

$$U \frac{\partial U}{\partial X} + V \frac{\partial U}{\partial Y} = -\frac{\partial P}{\partial X} + \frac{\nu_{nf}}{\nu_f} \cdot \frac{1}{Re} \nabla^2 U \tag{2.13}$$

$$U \frac{\partial V}{\partial X} + V \frac{\partial V}{\partial Y} = -\frac{\partial P}{\partial Y} + \frac{\nu_{nf}}{\nu_f} \nabla^2 V + Ri \frac{\beta_{nf}}{\beta_f} \theta \tag{2.14}$$

Energy equations

$$U \frac{\partial \theta}{\partial X} + V \frac{\partial \theta}{\partial Y} = \frac{1}{Re \, Pr} \frac{\alpha_{nf}}{\alpha_f} \nabla^2 \theta \tag{2.15}$$

For solid obstacle the energy equation is

$$\nabla^2 \theta_s + Q = 0 \tag{2.16}$$

The non-dimensional numbers that appear in equations (2.13)-(2.15) are as follows:

Reynolds number $Re = \frac{U_0 L}{\nu}$, Prandtl number $Pr = \frac{\nu}{\alpha}$, Richardson number $Ri = \frac{g\beta \, \Delta T \, L}{U_0^2}$.

25

2.2.4 Boundary conditions (non-dimensional form)

For case I:

At sliding double leads: $U = 0, V = 1, \theta = 0$

At horizontal top and bottom walls: $U = V = 0, \frac{\partial\theta}{\partial N} = 0$

At square block boundaries: $U = V = 0, \theta = 1$

At fluid solid interface: $\left(\frac{\partial\theta}{\partial N}\right)_{fluid} = K \left(\frac{\partial\theta_S}{\partial N}\right)_{solid}$

For case II:

At horizontal top wall: $U = -1, V = 0, \frac{\partial\theta}{\partial N} = 0$

At horizontal bottom wall: $U = 1, V = 0, \frac{\partial\theta}{\partial N} = 0$

At the vertical walls: $U = 0, V = 0, \theta = 0$

At square block boundaries: $U = V = 0, \theta = 1$

At fluid solid interface: $\left(\frac{\partial\theta}{\partial N}\right)_{fluid} = K \left(\frac{\partial\theta_S}{\partial N}\right)_{solid}$

where N is the non-dimensional distances either in X or Y direction acting normal to the surface and K is the ratio of the solid fluid thermal conductivity K_s/K_{nf} .

The average Nusselt number at the heated wall of the cavity based on the conduction

contribution may be expressed as $Nu = -\frac{1}{L}\int\limits_0^L \left(\frac{k_{nf}}{k_f}\right)\frac{\partial\theta}{\partial N}\ dN$ (2.17)

The average temperature and average velocity may be expressed as:

$\theta_{av} = \int \theta \, d\bar{V}/\bar{V}$ where L is the non-dimensional length of the surface.

The relationships between stream function ψ and velocity components U, V for two-dimensional flows are

$U = \frac{\partial\psi}{\partial Y}$ and $V = -\frac{\partial\psi}{\partial X}$ which give a single equation $\frac{\partial^2\psi}{\partial X^2} + \frac{\partial^2\psi}{\partial Y^2} = \frac{\partial U}{\partial Y} - \frac{\partial V}{\partial X}$.

The no-slip condition is valid at all boundaries as there is no cross-flow. Hence $\psi = 0$ is used for boundaries.

The heat flow within the enclosure is displayed using the heat function Π obtained from conductive heat fluxes $\left(-\dfrac{\partial\theta}{\partial X}, -\dfrac{\partial\theta}{\partial Y}\right)$ as well as convective heat fluxes $(U\theta, V\theta)$. The heat function satisfies the steady energy balance equation $\dfrac{\partial\Pi}{\partial Y} = U\theta - \dfrac{\partial\theta}{\partial X}$ and $-\dfrac{\partial\Pi}{\partial X} = V\theta - \dfrac{\partial\theta}{\partial Y}$ which yield a single equation $\dfrac{\partial^2\Pi}{\partial X^2} + \dfrac{\partial^2\Pi}{\partial Y^2} = \dfrac{\partial}{\partial Y}(U\theta) - \dfrac{\partial}{\partial X}(V\theta).$

2.3 Numerical Analysis

The governing equations along with the boundary conditions are solved numerically, employing Galerkin weighted residual finite element techniques discussed below.

2.3.1 Finite element formulation and computational procedure

To derive the finite element equations, the method of weighted residuals Zienkiewicz and Taylor [48] is applied to the equations (2.12) – (2.16) as

$$\int_A N_\alpha\left(\frac{\partial U}{\partial X} + \frac{\partial V}{\partial Y}\right)dA = 0 \tag{2.18}$$

$$\int_A N_\alpha\left(U\frac{\partial U}{\partial X} + V\frac{\partial U}{\partial Y}\right)dA = -\int_A H_\lambda\left(\frac{\partial P}{\partial X}\right)dA +$$
$$\frac{v_{nf}}{v_f}\frac{1}{Re}\int_A N_\alpha\left(\frac{\partial^2 U}{\partial X^2} + \frac{\partial^2 U}{\partial Y^2}\right)dA \tag{2.19}$$

$$\int_A N_\alpha\left(U\frac{\partial V}{\partial X} + V\frac{\partial V}{\partial Y}\right)dA = -\int_A H_\lambda\left(\frac{\partial P}{\partial Y}\right)dA + \frac{v_{nf}}{v_f}\int_A N_\alpha\left(\frac{\partial^2 V}{\partial X^2} + \frac{\partial^2 V}{\partial Y^2}\right)dA$$
$$+Ri\frac{\beta_{nf}}{\beta_f}\int_A N_\alpha\theta dA \tag{2.20}$$

$$\int_A N_\alpha\left(U\frac{\partial\theta}{\partial X} + V\frac{\partial\theta}{\partial Y}\right)dA = \frac{\alpha_{nf}}{\alpha_f}\frac{1}{Re\,Pr}\int_A N_\alpha\left(\frac{\partial^2\theta}{\partial X^2} + \frac{\partial^2\theta}{\partial Y^2}\right)dA \tag{2.21}$$

$$\int_A N_\alpha\left(U\frac{\partial\theta_s}{\partial X} + V\frac{\partial\theta_s}{\partial Y}\right)dA + \int_A N_\alpha Q\,dA = 0 \tag{2.22}$$

where A is the element area, N_α (α = 1, 2, … … , 6) are the element interpolation functions for the velocity components and the temperature and H_λ (λ = 1, 2, 3) are the element interpolation functions for the pressure.

Then apply Gauss's theorem into equations (2.19)-(2.22) to generate the boundary integral terms associated with the surface tractions and heat flux. After that the equations (2.19)-(2.22) become

$$\int_A N_\alpha \left(U \frac{\partial U}{\partial X} + V \frac{\partial U}{\partial Y} \right) dA + \int_A H_\lambda \left(\frac{\partial P}{\partial X} \right) dA +$$

$$\frac{v_{nf}}{v_f} \frac{1}{Re} \int_A \left(\frac{\partial N_\alpha}{\partial X} \frac{\partial U}{\partial X} + \frac{\partial N_\alpha}{\partial Y} \frac{\partial U}{\partial Y} \right) dA = \int_{S_0} N_\alpha S_x dS_0 \qquad (2.23)$$

$$\int_A N_\alpha \left(U \frac{\partial V}{\partial X} + V \frac{\partial V}{\partial Y} \right) dA + \int_A H_\lambda \left(\frac{\partial P}{\partial Y} \right) dA +$$

$$\frac{v_{nf}}{v_f} \int_A \left(\frac{\partial N_\alpha}{\partial X} \frac{\partial V}{\partial X} + \frac{\partial N_\alpha}{\partial Y} \frac{\partial V}{\partial Y} \right) dA - Ri \frac{\beta_{nf}}{\beta_f} \int_A N_\alpha \theta \, dA = \int_{S_0} N_\alpha S_y dS_0 \qquad (2.24)$$

$$\int_A N_\alpha \left(U \frac{\partial \theta}{\partial X} + V \frac{\partial \theta}{\partial Y} \right) dA + \frac{\alpha_{nf}}{\alpha_f} \frac{1}{Re \, Pr} \int_A \left(\frac{\partial N_\alpha}{\partial X} \frac{\partial \theta}{\partial X} + \frac{\partial N_\alpha}{\partial Y} \frac{\partial \theta}{\partial Y} \right) dA$$

$$= \int_{S_w} N_\alpha q_{1w} \, dS_w \qquad (2.25)$$

$$\int_A \left(\frac{\partial N_\alpha}{\partial X} \frac{\partial \theta_s}{\partial X} + \frac{\partial N_\alpha}{\partial Y} \frac{\partial \theta_s}{\partial Y} \right) dA + \int_A N_\alpha Q dA = \int_{S_w} N_\alpha q_{2w} \, dS_w \qquad (2.26)$$

The equations (2.23)-(2.24) specify surface tractions (S_x, S_y) along outflow boundary S_0 and (2.25)-(2.26) specifying velocity components and fluid temperature or heat flux (q_w) that flows into or out from domain along wall boundary S_w.

The basic unknowns for the above differential equations are the velocity components U, V, the temperature θ, θ_s and the pressure P. The six node triangular element is used in this work for the development of the finite element equations. All six nodes are associated with velocities as well as temperature; only the corner nodes are associated with pressure. This means that a lower order polynomial is chosen for pressure and which is satisfied through continuity equation.

The velocity component and the temperature distributions and linear interpolation for the pressure distribution according to their highest derivative orders in the differential equations (2.12)-(2.16) as

$$U(X,Y) = N_\beta U_\beta \tag{2.27}$$

$$V(X,Y) = N_\beta V_\beta \tag{2.28}$$

$$\theta(X,Y) = N_\beta \theta_\beta \tag{2.29}$$

$$\theta_s(X,Y) = N_\beta \theta_{s\beta} \tag{2.30}$$

$$P(X,Y) = H_\lambda P_\lambda \tag{2.31}$$

where $\beta = 1, 2, \ldots \ldots, 6;\ \lambda = 1, 2, 3.$

Substituting the element velocity component distributions, the temperature distribution, and the pressure distribution from equations (2.27)-(2.31), we get the following equations:

$$\int_A N_\alpha \left(N_{\beta,x} U_\beta + N_{\beta,y} V_\beta \right) dA = 0 \tag{2.32}$$

$$\int_A N_\alpha \left[\left(N_\beta U_\beta \right)\left(N_{\gamma,x} U_\gamma \right) + \left(N_\beta V_\beta \right)\left(N_{\gamma,y} U_\gamma \right) \right] dA + \int_A H_\lambda H_{\mu,x} P_\mu\, dA +$$
$$\frac{v_{nf}}{v_f} \frac{1}{Re} \int_A \left(N_{\alpha,x} N_{\beta,x} U_\beta + N_{\alpha,y} N_{\beta,y} U_\beta \right) dA = \int_{S_0} N_\alpha S_x\, dS_0 \tag{2.33}$$

$$\int_A N_\alpha \left[\left(N_\beta U_\beta \right)\left(N_{\gamma,x} V_\gamma \right) + \left(N_\beta V_\beta \right)\left(N_{\gamma,y} V_\gamma \right) \right] dA + \int_A H_\lambda H_{\mu,y} P_\mu\, dA +$$
$$\frac{v_{nf}}{v_f} \frac{1}{Re} \int_A \left(N_{\alpha,x} N_{\beta,x} V_\beta + N_{\alpha,y} N_{\beta,y} V_\beta \right) dA$$
$$- Ri \frac{\beta_{nf}}{\beta_f} \int_A N_\alpha N_\beta \theta_\beta\, dA = \int_{S_0} N_\alpha S_y\, dS_0 \tag{2.34}$$

$$\int_A N_\alpha \left[\left(N_\beta U_\beta \right)\left(N_{\gamma,x} \theta_\gamma \right) + \left(N_\beta V_\beta \right)\left(N_{\gamma,y} \theta_\gamma \right) \right] dA$$
$$+ \frac{\alpha_{nf}}{\alpha_f} \frac{1}{Re\, Pr} \int_A \left(N_{\alpha,x} N_{\beta,x} \theta_\beta + N_{\alpha,y} N_{\beta,y} \theta_\beta \right) dA = \int_{S_w} N_\alpha q_{1w}\, dS_w \tag{2.35}$$

$$\int_A N_\alpha \left[\left(N_\beta U_\beta \right)\left(N_{\gamma,x} \theta_{s\gamma} \right) + \left(N_\beta V_\beta \right)\left(N_{\gamma,y} \theta_{s\gamma} \right) \right] dA$$
$$+ \int_A N_\alpha Q \, dA = \int_{S_w} N_\alpha q_{2w} \, dS_w \tag{2.36}$$

Then the finite element equations can be written in the form

$$K_{\alpha\beta^x} U_\beta + K_{\alpha\beta^y} V_\beta = 0 \tag{2.37}$$

$$K_{\alpha\beta\gamma^x} U_\beta U_\gamma + K_{\alpha\beta\gamma^y} V_\beta U_\gamma + M_{\lambda\mu^x} P_\mu + \left(\frac{\nu_{nf}}{\nu_f} \frac{1}{Re} \right) \left(S_{\alpha\beta^{xx}} + S_{\alpha\beta^{yy}} \right) U_\beta = Q_{\alpha^u} \tag{2.38}$$

$$K_{\alpha\beta\gamma^x} U_\beta V_\gamma + K_{\alpha\beta\gamma^y} V_\gamma V_\gamma + M_{\alpha\mu^y} P_\mu + \left(\frac{\nu_{nf}}{\nu_f} \right) \left(S_{\alpha\beta^{xx}} + S_{\alpha\beta^{yy}} \right) V_\beta$$
$$- Ri \frac{\beta_{nf}}{\beta_f} K_{\alpha\beta} \theta_\beta = Q_{\alpha^v} \tag{2.39}$$

$$K_{\alpha\beta\gamma^x} U_\beta \theta_\gamma + K_{\alpha\beta\gamma^y} V_\beta \theta_\gamma + \left(\frac{\alpha_{nf}}{\alpha_f} \frac{1}{Re \, Pr} \right) \left(S_{\alpha\beta^{xx}} + S_{\alpha\beta^{yy}} \right) \theta_\beta = Q_{\alpha^\theta} \tag{2.40}$$

$$\left(S_{\alpha\beta^{xx}} + S_{\alpha\beta^{yy}} \right) \theta_{s\beta} + K_\alpha Q = Q_{\alpha^\theta}_s \tag{2.41}$$

where the coefficients in element matrices are in the form of the integrals over the element area and along the element edges S_0 and S_w as

$$K_{\alpha\beta^x} = \int_A N_\alpha N_{\beta,x} dA \tag{2.42a}$$

$$K_{\alpha\beta^y} = \int_A N_\alpha N_{\beta,y} dA \tag{2.42b}$$

$$K_{\alpha\beta\gamma^x} = \int_A N_\alpha N_\beta N_{\gamma,x} dA \tag{2.42c}$$

$$K_{\alpha\beta\gamma^y} = \int_A N_\alpha N_\beta N_{\gamma,y} dA \tag{2.42d}$$

$$K_{\alpha\beta} = \int_A N_\alpha N_\beta dA \tag{2.42e}$$

$$S_{\alpha\beta^{xx}} = \int_A N_{\alpha,x} N_{\beta,x} dA \tag{2.42f}$$

$$S_{\alpha\beta^{yy}} = \int_A N_{\alpha,y} N_{\beta,y} dA \tag{2.42g}$$

$$M_{\lambda\mu^x} = \int_A H_\lambda H_{\mu,x} dA \qquad (2.42\text{h})$$

$$M_{\alpha\mu^y} = \int_A H_\alpha H_{\mu,y} dA \qquad (2.42\text{i})$$

$$Q_{\alpha^u} = \int_{S_0} N_\alpha S_x dS_0 \qquad (2.42\text{j})$$

$$Q_{\alpha^v} = \int_{S_0} N_\alpha S_y dS_0 \qquad (2.42\text{k})$$

$$Q_{\alpha^\theta} = \int_{S_w} N_\alpha q_{1w} dS_w \qquad (2.42l)$$

$$Q_{\alpha^\theta_s} = \int_{S_w} N_\alpha q_{2w} dS_w \qquad (2.42\text{m})$$

$$K_\alpha = \int_A N_\alpha dA \qquad (2.42\text{n})$$

These element matrices are evaluated in closed form ready for numerical simulation. Details of the derivation for these element matrices are omitted herein.

For numerical simulation, these element matrices are evaluated in closed-form. Details of the derivation for these element matrices are omitted herein for briefness.

The resultant finite element equations (2.37)-(2.41), are nonlinear. These nonlinear algebraic equations are solved employing the Newton-Raphson iteration technique by first writing the unbalanced values from the set of the finite element equations (2.37)-(2.41) as,

$$F_{\alpha^p} = K_{\alpha\beta^x} U_\beta + K_{\alpha\beta^y} V_\beta \qquad (2.43\text{a})$$

$$
\begin{aligned}
F_{\alpha^u} = {} & K_{\alpha\beta\gamma^x} U_\beta U_\gamma + K_{\alpha\beta\gamma^y} V_\gamma U_\gamma + M_{\alpha\mu^x} P_\mu \\
& + \left(\frac{\nu_{nf}}{\nu_f} \frac{1}{Re} \right) (S_{\alpha\beta^{xx}} + S_{\alpha\beta^{yy}}) U_\beta - Q_{\alpha^u}
\end{aligned}
\qquad (2.43\text{b})
$$

$$
\begin{aligned}
F_{\alpha^v} = {} & K_{\alpha\beta\gamma^x} U_\beta V_\gamma + K_{\alpha\beta\gamma^y} V_\gamma V_\gamma + M_{\alpha\mu^y} P_\mu + \left(\frac{\nu_{nf}}{\nu_f} \right) (S_{\alpha\beta^{xx}} + S_{\alpha\beta^{yy}}) V_\beta \\
& - Ri \frac{\beta_{nf}}{\beta_f} K_{\alpha\beta} \theta_\beta - Q_{\alpha^v}
\end{aligned}
\qquad (2.43\text{c})
$$

$$F_{\alpha^\theta} = K_{\alpha\beta\gamma^x} U_\beta \theta_\gamma + K_{\alpha\beta\gamma^y} V_\beta \theta_\gamma + \frac{\alpha_{nf}}{\alpha_f} \frac{1}{Re\,Pr} \left(S_{\alpha\beta^{xx}} + S_{\alpha\beta^{yy}} \right) \theta_\beta - Q_{\alpha^\theta} \qquad (2.43\text{d})$$

$$F_{\alpha\theta_s} = \left(S_{\alpha\beta^{xx}} + S_{\alpha\beta^{yy}} \right) \theta_{s\beta} + K_\alpha Q - Q_{\alpha\theta_s} \tag{2.43e}$$

This leads to a set of algebraic equations with the incremental unknowns of the element nodal velocity components, temperatures, and pressures in the form,

$$\begin{bmatrix} K_{uu} & K_{uv} & K_{u\theta} & K_{up} & 0 \\ K_{vu} & K_{vv} & K_{v\theta} & K_{vp} & 0 \\ K_{\theta u} & K_{\theta v} & K_{\theta\theta} & 0 & 0 \\ K_{pu} & K_{pv} & 0 & 0 & 0 \\ 0 & 0 & 0 & 0 & K_{\theta_s\theta_s} \end{bmatrix} \begin{bmatrix} \Delta u \\ \Delta v \\ \Delta\theta \\ \Delta p \\ \Delta\theta_s \end{bmatrix} = \begin{bmatrix} F_{\alpha^u} \\ F_{\alpha^v} \\ F_{\alpha\theta} \\ F_{\alpha^p} \\ F_{\alpha\theta_s} \end{bmatrix} \tag{2.44}$$

where $K_{uu} = K_{\alpha\beta\gamma^x} U_\beta + K_{\alpha\beta\gamma^x} U_\gamma + K_{\alpha\beta\gamma^y} V_\beta + \left(\dfrac{\nu_{nf}}{\nu_f} \dfrac{1}{Re} \right) \left(S_{\alpha\beta^{xx}} + S_{\alpha\beta^{yy}} \right)$

$K_{uv} = K_{\alpha\beta\gamma^y} U\gamma$

$K_{u\theta} = K_{u\theta_s} = 0$

$K_{up} = M_{\alpha\mu^x}$

$K_{vu} = K_{\alpha\beta\gamma^x} V\gamma$

$K_{vv} = K_{\alpha\beta\gamma^x} U_\beta + K_{\alpha\gamma\beta^y} V_\gamma + K_{\alpha\beta\gamma^y} V_\gamma + \left(\dfrac{\nu_{nf}}{\nu_f} \dfrac{1}{Re} \right) \left(S_{\alpha\beta^{xx}} + S_{\alpha\beta^{yy}} \right)$

$K_{v\theta} = -Ri \dfrac{\beta_{nf}}{\beta_f} K_{\alpha\beta}$

$K_{vp} = M_{\alpha\mu^y}, \quad K_{v\theta_s} = 0$

$K_{\theta u} = K_{\alpha\beta\gamma^x} \theta\gamma$

$K_{\theta v} = K_{\alpha\beta\gamma^y} \theta\gamma$

$$K_{\theta\theta} = K_{\alpha\beta\gamma^x} U_\beta + K_{\alpha\beta\gamma^y} V_\beta + \frac{\alpha_{nf}}{\alpha_f} \frac{1}{Re\,Pr} (S_{\alpha\beta^{xx}} + S_{\alpha\beta^{yy}})$$

$$K_{\theta p} = K_{\theta\theta_s} = 0$$

$$K_{pu} = M_{\alpha\mu^x}$$

$$K_{pv} = M_{\alpha\mu^y}$$

$$K_{p\theta} = K_{pp} = K_{p\theta_s} = 0$$

$$K_{\theta_s u} = K_{\theta_s v} = K_{\theta_s p} = K_{\theta_s \theta} = 0$$

$$K_{\theta_s \theta_s} = \left(S_{\alpha\beta^{xx}} + S_{\alpha\beta^{yy}} \right)$$

The iteration process is terminated if the percentage of the overall change compared to the previous iteration is less than the specified value.

To solve the sets of the global nonlinear algebraic equations in the form of matrix, the Newton-Raphson iteration technique has been adapted through PDE solver with MATLAB interface. The convergence of solutions is assumed when the relative error for each variable between consecutive iterations is recorded below the convergence criterion ε such that

$\left| \Psi^{n+1} - \Psi^n \right| < \varepsilon$, where n is number of iteration and $\Psi = U, V, \theta$. The convergence criterion was set to 10^{-5}.

2.3.2 Grid size sensitivity test

In this chapter a lid driven cavity is considered as the geometry, therefore several grid size sensitivity tests are conducted in this geometry to determine the sufficiency of the mesh scheme and to ensure that the solutions are grid independent. Therefore a grid independence study was executed to make sure the correctness of the numerical results for a square cavity at the representative value of $Pr = 6.2$, $Re = 100$, $K = 5$, $Ri = 1$, $Q = 1$ and $\chi = 0.05$. Non-uniform triangular element grid system is employed in the present study.

The extreme value of Nu_{av} is used as a sensitivity measure of the accuracy of the solution and is selected as the monitoring variable considering both the accuracy of numerical value and computational time. This is described in Figure 2.2. It is observed that the magnitude of the average Nusselt number for 10843 elements shows a very little difference with the results obtained for the other higher elements. The element 10843 is chosen for further calculation. This grid resolution is therefore used for all consequent calculations.
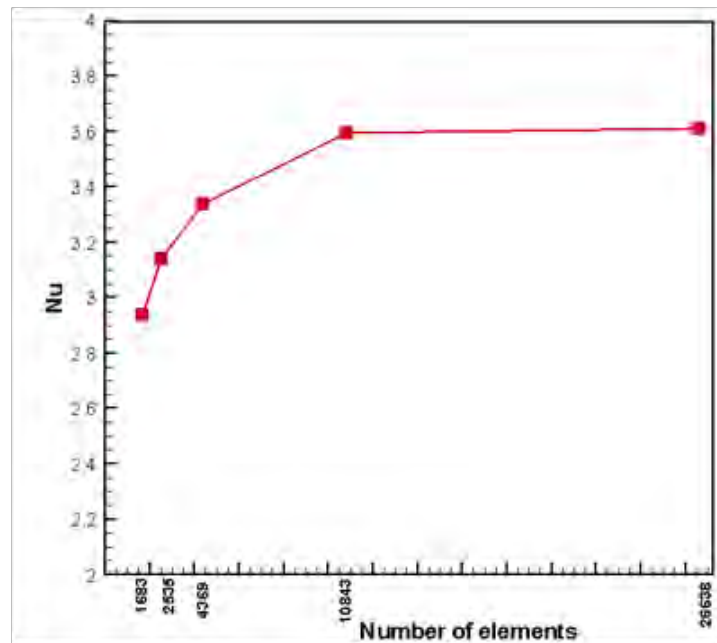
Figure 2.2: Grid sensitivity test while Pr = 6.2, Re = 100, K = 5, Ri = 1, Q = 1 and χ = 0.05.

2.3.3 Validation of the numerical scheme

In order to verify the accuracy of the numerical results and the validity of the mathematical model obtained throughout the present study, comparisons with the previously published results are essential. But due to the lack of availability of experimental data on the particular problems along with its associated boundary conditions investigated in this study, validation of the predictions could not be done against experiment.

The present numerical model is verified for heat transfer and flow characteristics for MHD mixed convection in a lid-driven cavity with heat generating obstacle by Billah et al. (2011). However, we recall here some results obtained by our model in comparison with those reported in Billah et al. (2011) for Re = 100, Ha = 10, Q = 1, Pr = 0.71, Ri = 10 and K = 5.

Billah et. al (2011)   Present work
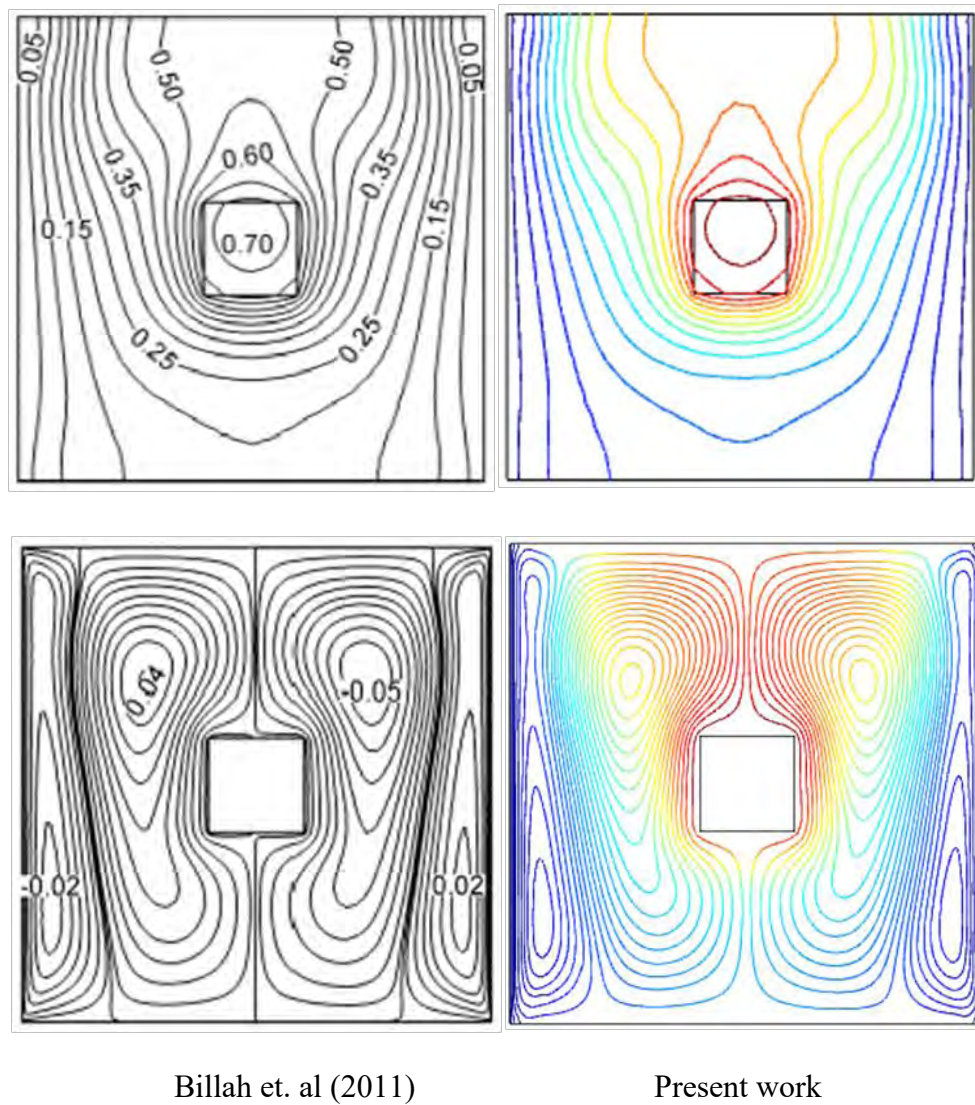
Figure 2.3: Comparison of the present work with Billah et al. (2011) while Re = 100, Ha = 10, Q = 1, Pr = 0.71, Ri = 10 and K = 5 for isotherms (top) and streamlines (bottom).

The physical problem studied by Billah et al. (2011) was a lid-driven enclosure with sides of length L. A heat generating solid square obstacle is positioned at the center of the cavity. In addition, the cavity is saturated with electrically conducting fluid. The solid obstacle has a thermal conductivity of k_s and generates uniform heat flux (q) per unit area. Moreover, the vertical walls of the cavity are mechanically lid-driven and considered to be at a constant temperature T_c and uniform velocity V_0 in the positive y direction (upward). Furthermore, both the top and bottom surfaces of the enclosure are kept adiabatic. The uniform magnetic field of strength B_0 is applied in the horizontal direction.

Finally, the streamlines and isotherms for Re = 100, Ha = 10, Q = 1, Pr = 0.71, Ri = 10 and K = 5 is presented in the Figure 2.3. It can be seen from the figure that the present results and those of Billah et al. (2011) are in excellent agreement. This validation boosts the confidence in the numerical outcome of the present work.

CHAPTER 3
RESULTS AND DISCUSSION

The present numerical study is carried out for Al_2O_3-water nanofluid with the help of finite-element method. The current investigation is to explore the conjugate effects of nanofluids on mixed convection heat transfer in a square cavity in the presence of heat generating object in heatline approach. Numerical results are presented in order to determine the effects of the presence of dimensionless parameters. The dimensionless parameters that must be specified for the system are Reynolds number (Re), solid fluid thermal conductivity ratio (K), Richardson number (Ri), heat generation parameter (Q) and solid volume fraction (χ). Results are presented in terms of isotherms, streamlines and heatlines contours along with necessary plots at different values of Re, K, Ri, Q and χ for case I and II. Representative distributions of average Nusselt number (Nu_{av}) at the heated surface, the dimensionless average temperature θ_{av} of the fluid and the solid, maximum average temperature of the fluid and solid and the average heat flux magnitude will be presented.

3.1 Effect of Reynolds Number

Mixed convection flow for nanofluid inside a lid driven cavity having a heat generating square obstacle is governed by different parameter namely Prandtl number Pr, Reynolds number Re, solid volume thermal conductivity ratio K, Richardson number Ri, heat generation parameter Q and solid volume fraction χ. Here the Reynolds number Re is involved to control the heat transfer and fluid flow in this section and the other parameters are kept fixed at Pr = 6.2, K = 5, Ri = 1, Q = 1, and χ = 0.05. The results are presented in terms of isotherms, streamlines and heatlines pattern. Figure 3.1(a) is showing the isotherms for different values of Reynolds number from 20 to 150 (case I). Here the color indicates the temperature of the flow field, blue is for lower temperature and red color indicates higher temperature. The higher valued isothermal lines are near the heat generating object and lower valued lines are near the side walls. For Re = 20 the isotherms near the upper boundary are looked like the shadow of human arms. From the figure it can

be said that when Re increases that is the inertia force increases due to the movement of two vertical lids the isothermal lines near the upper boundary become sharp and near the heat generating obstacle these are more condensed. For Re = 100 and 150 the isotherm disappears near the upper boundary and number of isotherms increase which indicates higher temperature gradient. A thermal plume is developed near the vertical wall for higher values of Re.

The flow field inside a double lid driven cavity with heat generating object in terms of computed streamlines for various Reynolds number is shown in figure 3.1(b). The other parameters are kept fixed at Pr = 6.2, K = 5, Ri = 1, Q = 1, and χ = 0.05. Here the color indicates the velocity magnitude of the flow field, blue to red means lower to higher velocity. Due to the upward motion of the vertical walls, fluid rises up along the vicinity of the vertical walls forming clockwise rotating cell as well as anticlockwise rotating cell near the left and right vertical lids respectively for aforesaid values of Re. The flow strength increases for the increasing value of Re. The size of the vortex as well as the flow strength has a strong effect as the Re is increased from 20 to 150. The flow field is almost symmetrical adjacent of the side walls for all values of Re. For the given boundary condition there form two counter clockwise vortex at two sides of the cavity. For Re = 100 and 150, the stream lines are little bit away from the heat generating object near the bottom wall and become closer near the upper wall. The elliptic shape of the core of the vortex becomes circular as Reynolds number gets the higher values. If the Reynolds number is increased the vortex inside the cavity becomes slightly stronger which is a sign of supremacy of forced convection in the cavity.

The heat lines for various Reynolds number is shown figure 3.1(c). The figure shows the flow of the heat due to the mixed convection in a square cavity with a heat generating obstacle while the above mentioned parameters are kept fixed as the same value. Here the red color indicates the higher heat flux magnitude and the blue color indicates the lower heat flux magnitude. From the figure it can be said that there is well built effect of Re on heatline structure.

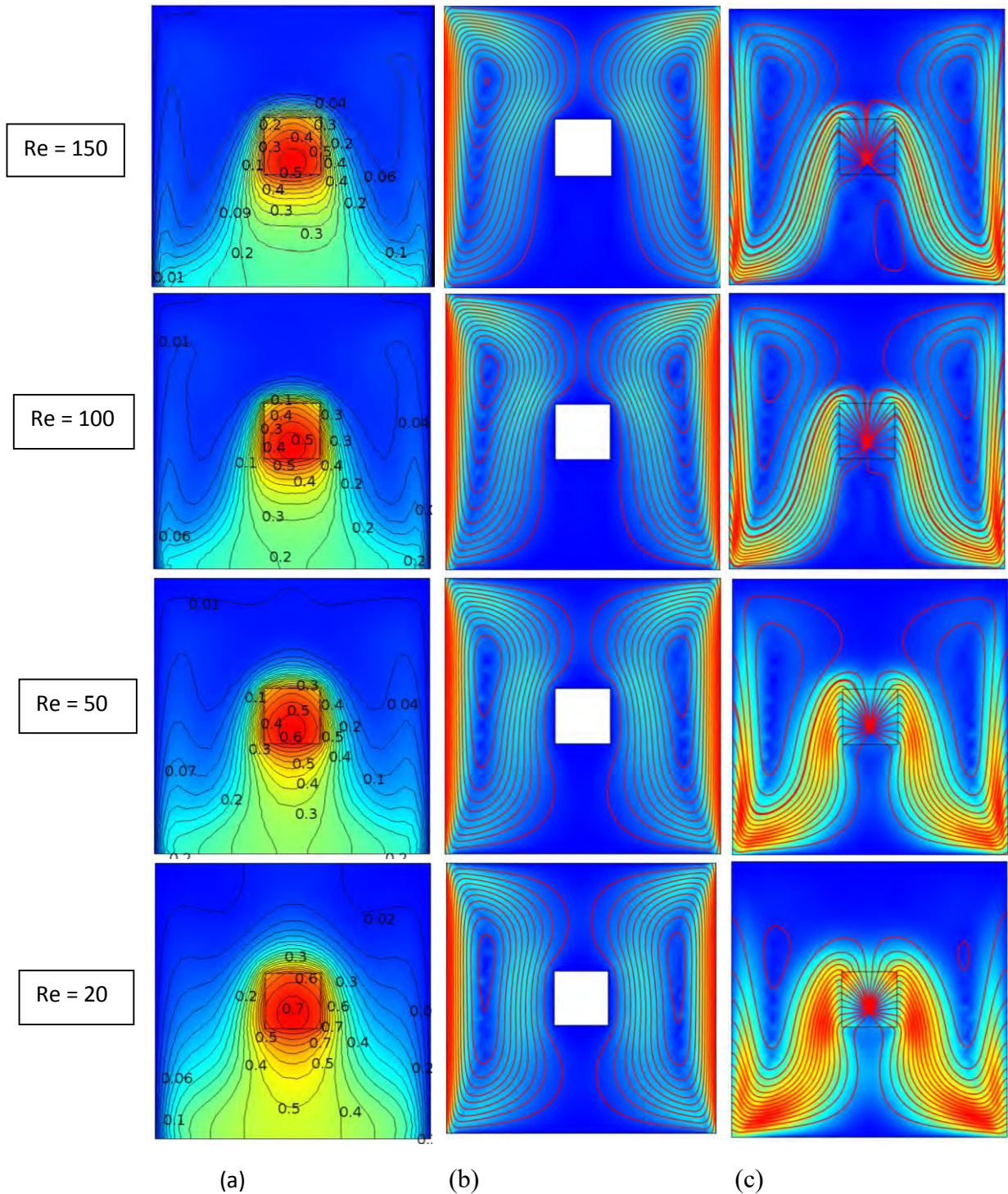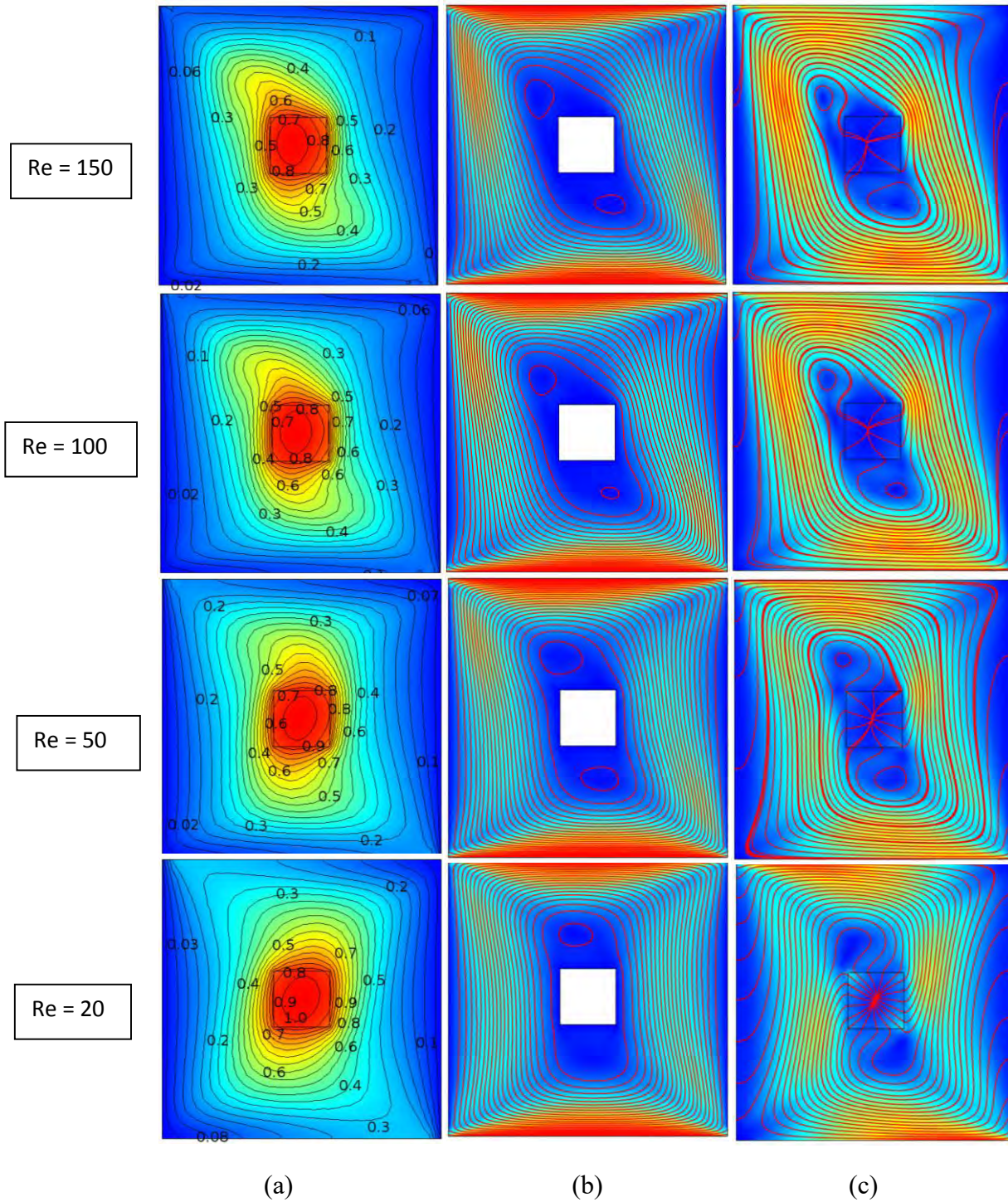**Figure 3.1:** (a) Isotherms, (b) streamlines and (c) heatlines for different values of Re (case I) with Pr = 6.2, K = 5, Ri = 1, Q = 1 and χ = 0.05.

Figure 3.2: (a) Isotherms, (b) streamlines and (c) heatlines for different values of Re (case II) with Pr = 6.2, K = 5, Ri = 1, Q = 1 and χ = 0.05.

The flow pattern is symmetric about vertical mid line. When Re = 20, the heatlines are denser near the side walls due to movement of the side walls and elliptic shape lines are less in number. When Re is increased from 20 to 50 it is found that the heatlines become denser near the heat generating obstacle due to forced convection. Also it is found that the elliptic heat lines increases near the side walls. In the next figure when Re is increases to 100 and 150, the orientation of the heatlines are almost similar. Since the fluid is water Al_2O_3 nanofluid and the forced convection becomes stronger that causes the heat transfer rate to increase. Therefore, at high Reynolds numbers addiction of nanoparticles motivates increase in heat transfer rate.

The effect of Reynolds number on the temperature distributions for the case II are illustrated in the figure 3.2 by plotting the isotherms, streamlines and heatlines, while the other parameters are kept fixed as Pr = 6.2, K = 5, Ri = 1, Q = 1 and χ = 0.05. The corresponding isotherms results from the figure indicates that obstacle remains at higher temperature. The lower valued isotherms are nearer the boundaries and the higher valued lines are nearer the heat generating object. At high Reynolds number the forced convection plays a dominant role, and the recirculation flow is mostly generated by the moving lid. We also observe that from the figure 3.2(a) as the Reynolds number enhances from 20 to 150, the temperature contours tend to get affected considerably. At Re = 20, the isothermal lines near the heat generating object are elliptic and slightly inclined to the right corner, the isothermal lines near the side walls are rectangular. When Re increases that is inertia force increases due to the movement of the upper and lower leads, it is observed that the isothermal lines are denser to the upper left corner since the upper lead is moving to the left with considerably higher velocity.

In figure 3.2(b), the streamlines are shown for different values of Reynolds number. At Re = 20 the flow strength of the nanofluid is symmetric about the vertical mid line. This is also observed for the other values of Reynolds number. Almost all the streamlines are rectangular in shape. But for the higher Reynolds number the direction of the motion of the fluid is affected by the movement of the upper and lower boundaries which is in counter clockwise direction. That is why the streamlines are denser for the higher values of Reynolds number. In figure 3.2(c), the heatline pattern is shown for different values of

Reynolds number while Pr = 6.2, K = 5, Ri = 1, Q = 1 and χ = 0.05. For low Reynolds number the heatlines are symmetric about the vertical mid line inside the domain. When the values of Reynolds number increases from 20 to 50 the heatlines is denser which is observed for the other values of Reynolds numbers and the heatlines overlap, which cause the heat transport through the fluid.

In figure 3.3, the effect of Reynolds number on average Nusselt number at the heat source, average fluid temperature in the cavity, maximum temperature in the cavity and the average heat flux magnitude for the cases I and II are presented while Pr = 6.2, K = 5, Ri = 1, Q = 1 and χ = 0.05. The average Nusselt number for the increasing value of Re slightly changed for both the cases and all the values of Nusselt number are apparently higher in case I than that of case II. The average temperature of the solid and fluid for case I and II are shown in the next figure where it is observed that the average temperature of the solid decreases for the increasing value of Re. The average temperature of the fluid decreases very slowly and after Re = 50 the average temperature is almost constant. The next figure is for maximum temperature for various values of Reynolds number. The maximum temperature for case I is lower than that of case II. Again average heat flux magnitude increases rapidly for the increasing value of Re while the heat flux magnitude increases very slowly for case I. Finally the quantitative measurements of average Nusselt number, average temperature, maximum temperature and the average heat flux magnitude are tabulated in the tables 3.1(a), 3.1(b), 3.1(c) and 3.1(d) respectively for the cases I and II with different Reynolds numbers.
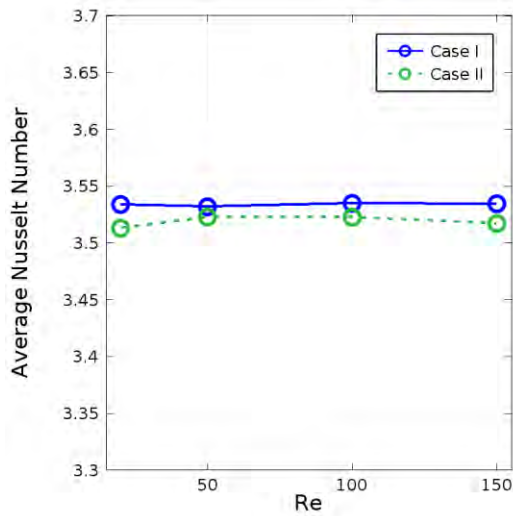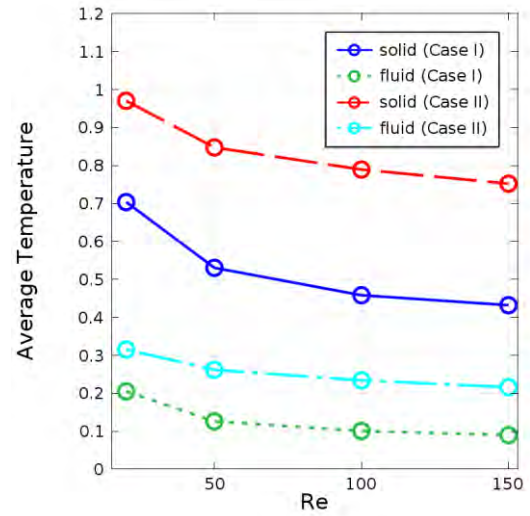
(a)   (b)
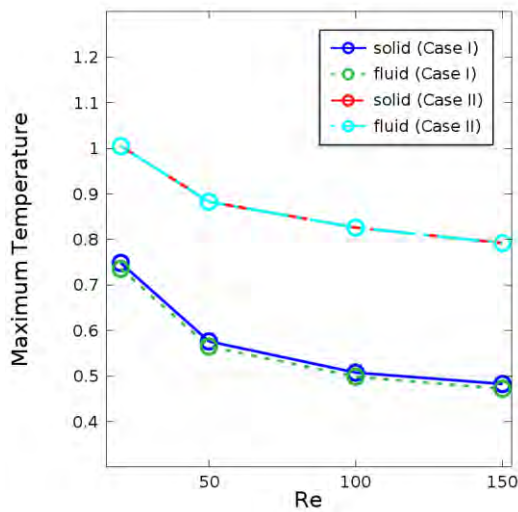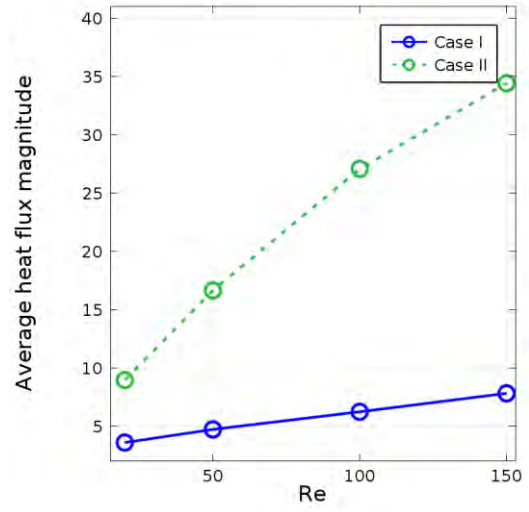
(c)   (d)

Figure 3.3 (a) Average Nusselt number, (b) average temperature of the solid and the fluid, (c) maximum temperature of the solid and the fluid and (d) average heat flux magnitude for different values of Re, with Pr = 6.2, K = 5, Ri = 1, Q = 1 and χ = 0.05.

Table 3.1 (a): Variation of average Nusselt number with Re

Re	Case I	Case II
20	3.53386	3.51295
50	3.53180	3.52286
100	3.53487	3.52267
150	3.53455	3.51710

Table 3.1 (b): Variation of average temperature with Re

Re	solid(case I)	fluid(case I)	solid(case II)	fluid(case II)
20	0.70384	0.20508	0.9706	0.31521
50	0.53062	0.12609	0.84769	0.26190
100	0.45834	0.10062	0.78953	0.23402
150	0.43213	0.08979	0.75228	0.21602

Table 3.1 (c): Variation of maximum temperature with Re

Re	solid(case I)	fluid(case I)	solid(case II)	fluid(case II)
20	0.74838	0.73557	1.00488	1.00488
50	0.57628	0.56492	0.88278	0.88278
100	0.50764	0.49861	0.82605	0.82605
150	0.48274	0.47218	0.79202	0.79202

Table 3.1 (d): Variation of average heat flux magnitude with Re

Re	Case I	Case II
20	3.60620	8.96568
50	4.73351	16.6571
100	6.24679	27.0822
150	7.82795	34.43532

3.2 Effect of Solid Fluid Thermal Conductivity Ratio

Cooling mechanism is one of the most important concerns in the industry. In most cases cooling improvement of existing heat exchanger is done by increasing the size of these systems which is not desirable. In recent years nanofluid is used to improve the heat transfer since it is with higher thermal conductivity than the pure fluid.

In the present problem, isotherms, streamlines and heatlines for case I are shown in figure 3.4 for various values of solid fluid thermal conductivity ratio K(0.2, 1,5 and 50) while the other parameters are kept fixed as Pr = 6.2, Re = 100, Ri = 1, Q = 1 and χ = 0.05. Now from the figure 3.4(a) it is a reminder that the thermal conductivity of the heat generating obstacle effects strongly on the isotherm structures. At the lower value of K = 0.2, the lower values isotherm near the heat-generating body is parabolic but higher values isothermal lines are elliptic. In addition, the thermal layer inside and on the boundary of heat generating square obstacle is more concentrated indicating most of the heat is concentrated inside and on the boundary of a heat generating body for the lowest value of K, because this body generates heat and contains more heat from the surrounding space. The concentrated isotherm reduces from the heat-generating obstacle with the increasing values of K since the thermal conductivity increases for the increasing value of K as a result the parabolic shaped isotherms increases. It is also observed that when K increases the isotherms near the side walls which occurs due to the movement of the side walls.

The flow field inside a double-lid driven square cavity in terms of computed streamline for the four representative values of the solid fluid thermal conductivity ratio K (= 0.2, 1, 5 and 50), while Pr = 6.2, Re = 100, Ri = 1, Q = 1 and χ = 0.05 is shown in figure 3.4(b). For all values of K the flow field becomes symmetrical about vertical wall. Now for K = 0.2, the fluid flow is characterized by a clockwise and anti-clockwise eddy generated by the motion of the vertical lids. Again for the different higher values of K (1.0, 5. and 50), it is evident that the size as well as the flow strength of the vortices remains unaffected with the increasing value of K. This behavior is rational because thermal conductivity of the solid has a negligible effect in the flow field. For all values of K the flow field becomes

symmetrical about vertical line due to the presence of double-lids having uniform velocity, temperature and direction.

The heatlines for various solid fluid thermal conductivity ratio are shown in the figure 3.4(c). From the figure it can easily be said that there is well built effect of K on heat line structure. Since heatlines represents the trajectory of the heat flow and the concept is similar to streamline, therefore a clockwise and anticlockwise direction is observed due to the movement of the side walls. Heat flux lines originated from the solid block becomes denser for higher values of K. If K increases then the heat flow increases since the thermal conductivity of the solid block is higher than that of nanofluid.

In the present case II, the isotherms, streamlines and heatlines are shown in figure 3.5 for various values of solid fluid thermal conductivity ratio K (0.2, 1, 5, 50) while the other parameters are kept fixed as Pr = 6.2, Re = 100, Ri = 1, Q = 1 and χ = 0.05. In the first column, figure 3.5(a) the isotherms are shown. The first figure is for K = 0.2 which is lowest value for the considered four values which shows that the isothermal lines are denser near the heat generating object. These isothermal lines are comparatively higher valued than those are near the boundaries. The isothermal lines nearer the heat generating object are elliptic and the lines nearer the upper and lower moving boundaries are seemed to be like rectangular due to the movement of the boundaries. The next figure is for K = 1 where the number of isothermal lines increases in the fluid domain. Like the previous case the isothermal lines near the heat generating body are elliptic, in the center they are almost circular and near the upper and lower moving walls the lines are rectangular. In the same manner for the next two values of solid fluid thermal conductivity ratio K (5 and 50), the conductivity of the heat generating body is higher and the isothermal lines increase and making a comparison of the isothermal lines for different values of *K,* no significant difference is found except shifting of the isothermal lines from the center of the heat-generating obstacle.

(a)   (b)   (c)

Figure 3.4: (a) Isotherms, (b) streamlines and (c) heatlines (case I) for different values of K with Pr = 6.2, Re = 100, Ri = 1, Q = 1 and χ = 0.05.

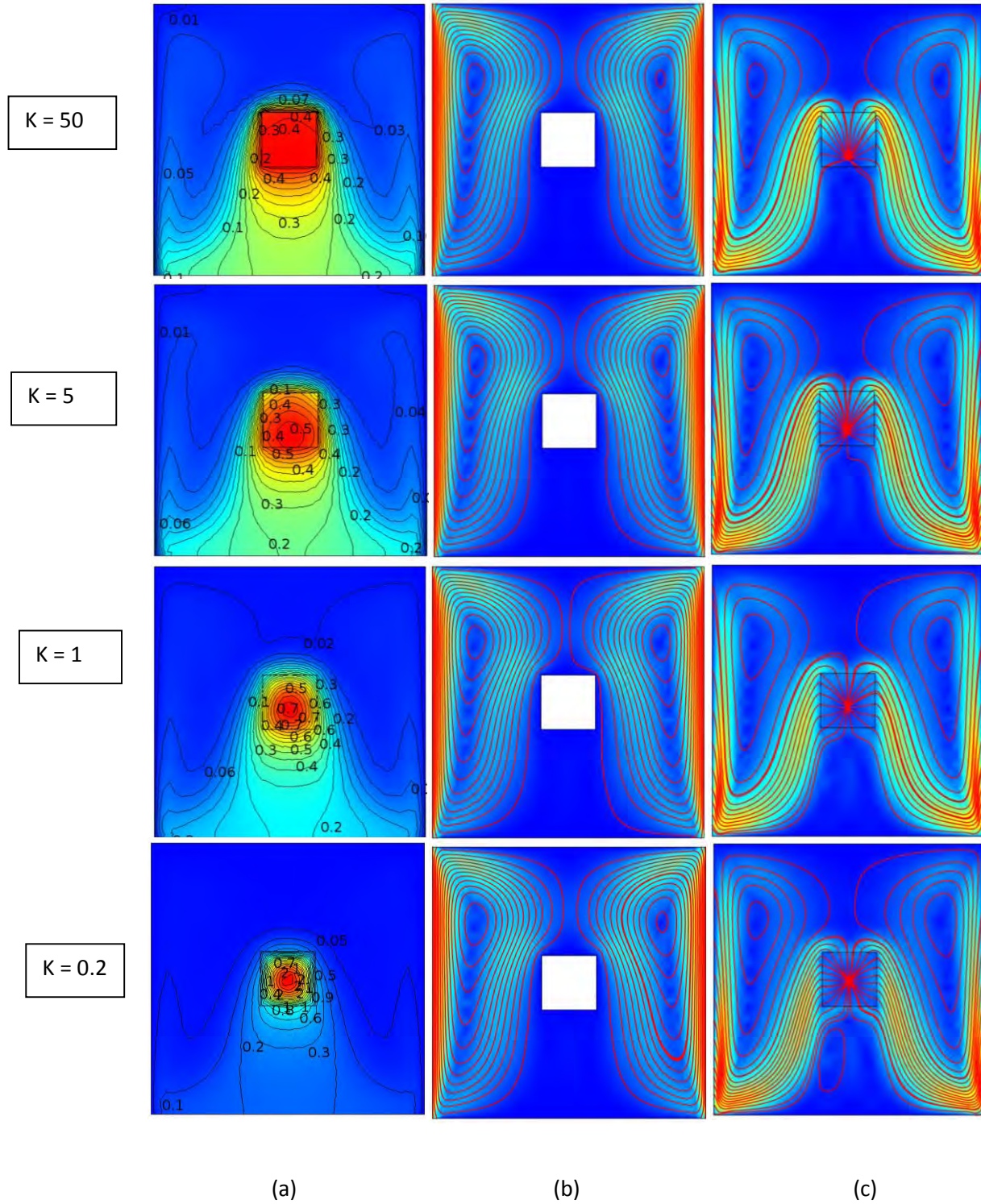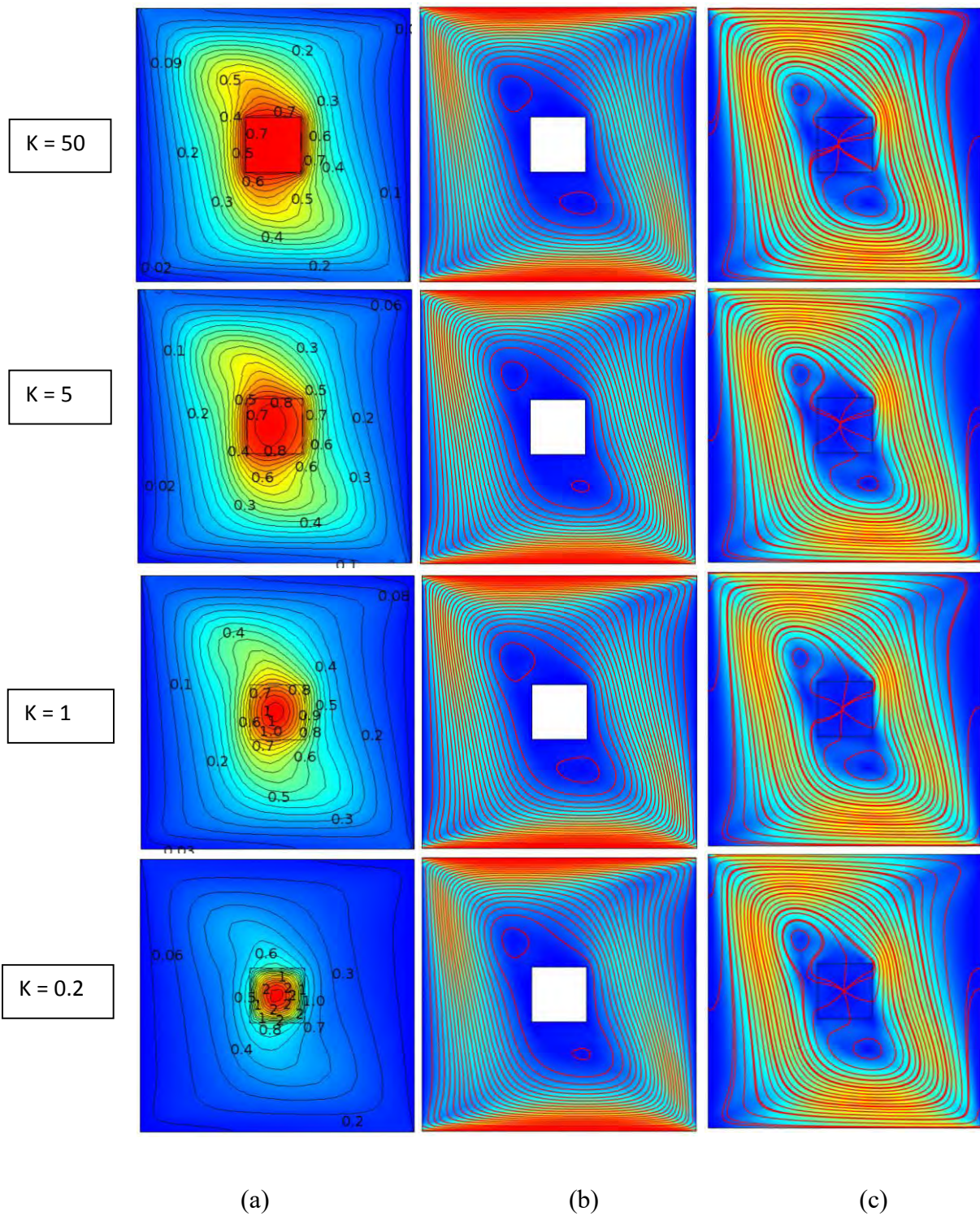**Figure 3.5:** (a) Isotherms, (b) streamlines and (c) heatlines (case II) for different values of K with Pr = 6.2, Re = 100, Ri = 1, Q = 1 and χ = 0.05.

In figure 3.5(b), streamlines for different values of solid fluid thermal conductivity ratio K (0.2, 1, 5, 50) are shown while the other parameters are kept fixed as Pr = 6.2, Re = 100, Ri = 1, Q = 1 and χ = 0.05. For K = 0.2, the streamlines are shown in the first figure. From the figure it can be said the direction of the streamlines are greatly affected by the movement of the upper and lower boundaries. For the other values of K (1, 5 and 50) the direction as well as the vortex of the motion remain the same as the previous value of K except the number of streamlines increase.

In the third column of figure 3.5 the heatlines for different of K are shown while the other parameters are kept fixed as Pr = 6.2, Re = 100, Ri = 1, Q = 1 and χ = 0.05. For different values of K there is very low effect on the heatline pattern. Here heat flow occurs mainly due to convection as the heatlines are nearly perpendicular to the isotherm lines as well the walls. Here the intensity of fluid circulations is found to be much stronger near the side walls specially near the upper and lower moving walls due to the movement of the walls. The large regime of the convection is due to the large amount of heat transport from the moving walls associated with the large intensity of circulation. Therefore if the values of K increases from 0.2 to 50 the heat flux lines also increases near the side walls and transports heat from the center to the side walls.

The effect of solid fluid thermal conductivity ratio on average Nusselt number at the heat source, average fluid temperature in the cavity, maximum temperature and the average heat flux magnitude are shown in the figure 3.6 for case I and II. The figure 3.6(a) shows the distribution of the average Nusselt number vs. the solid fluid thermal conductivity ratio K. for the both cases when K = 0.2, the average Nusselt number is very high. If K increases to 1 then there is a rapid decrease in the average Nusselt number. Thereafter the average Nusselt number decreases slowly for the next two values of K. From the figure it seems that for the above mentioned two cases all the values overlap that is there is similar changes for the values of K. In the figure 3.6(b) the variation of average temperature vs. K is shown for solid and fluid of case I and that of case II. It is observed that for both cases the average temperature of the fluid remain unchanged for various values of K (0.2, 1, 5 and 50). The result match with the result found in the streamline pattern for various values of K. The average temperature of the fluid for case II is higher than that of case I in every case.

(a)

(b)

(c)

(d)
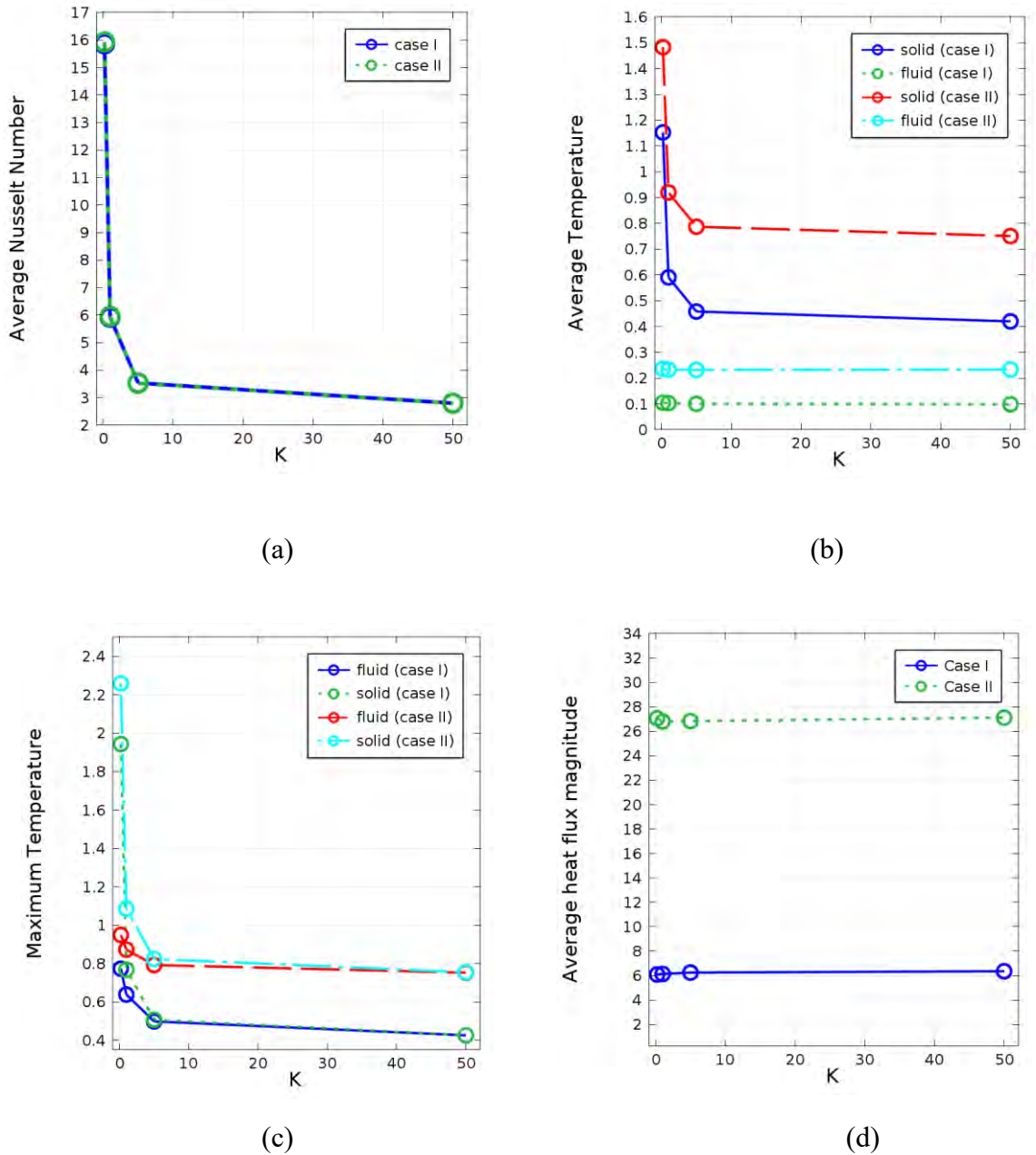
Figure 3.6: (a) Average Nusselt number , (b) average temperature of the solid and the fluid, (c) maximum temperature of the solid and the fluid and (d) average heat flux magnitude for different values of K, with Pr = 6.2, Re = 100, Ri = 1, Q = 1 and χ = 0.05.

Table 3.2 (a): Variation of average Nusselt number with K

K	Case I	Case II
0.2	15.86172	15.93062
1	5.92333	5.959422
5	3.53487	3.522612
50	2.80057	2.795242

Table 3.2 (b): Variation of average temperature with K

K	solid(case I)	fluid(case I)	solid(case II)	fluid(case II)
0.2	1.152742	0.10514	1.48286	0.23617
1	0.590852	0.10308	0.91973	0.23318
5	0.458322	0.10059	0.78707	0.23218
50	0.420082	0.09901	0.750877	0.23345

Table 3.2 (c): Variation of maximum temperature with K

K	fluid(case I)	solid(case I)	fluid(case II)	solid(case II)
0.2	0.77339	1.94317	0.94905	2.25902
1	0.63845	0.76805	0.87245	1.08629
5	0.498595	0.50763	0.792245	0.82358
50	0.426058	0.42633	0.752335	0.75483

Table 3.2 (d): Variation of average heat flux magnitude with K

K	Case I	Case II
0.2	6.08861	27.06434
1	6.13194	26.79185
5	6.24505	26.83165
50	6.35479	27.11632

Again the average temperature of the solid (case II) is higher than the average temperature of the solid (case I). For the lower values of K the average temperature is high and for the value of K from 5 to 50 the variation in the average temperature is very slow in both cases. The next figure is showing the maximum temperature of the solid and fluid in both cases. Maximum temperature of the solid for case I is higher than solid for case II. Also it can be said that the maximum temperature of the fluid (both cases) is a little bit higher for the lower value of K. The average heat flux magnitude for different values of K are shown in the figure 3.6(d) for case I and case II. Here it is observed that the average heat flux magnitude for case II is higher than that of case I. It is also observed that for the increasing value of K there is very small effect of average heat flux magnitude which is negligible. It is further observed that, although the variation of the average Nusselt number with K is qualitatively similar for the abovementioned cases, but has quantitatively dissimilarity, which are well documented in the Tables 3.2 (a), (b), (c) and (d).

3.3 Effect of Richardson Number

Figure 3.7 shows the results obtained for case I for various values of Richardson number in the form of isotherms, streamlines and heatlines. For case I, the upper and lower lids are adiabatic, left and right walls are moving upwards. These movements of the lids cause two primary vortices to be formed near the lids. According to the direction of the lids movement, the vortex which is formed by the force resulting from the movement of the left lid is clockwise and the vortex which is formed by the force resulting from movement of the right lid is counterclockwise. Richardson number in figure 3.7 is set to 0, 1 and 10 whether the other parameters are kept fixed as $Pr = 6.2$, $Re = 100$, $Q = 1$, $K = 5$ and $\chi = 0.05$. Here $Ri = 0$ stands for pure forced convection which means that the force due to movement of the lids dominates over the buoyancy force. The isotherms for Richardson number of 0, 1 and 10 are shown in the figure 3.7(a). At $Ri = 0$ the isotherms demonstrate that temperature gradient near the cold wall and particularly the hot wall is very high which shows high rate of heat transfer in these areas. In fact, temperature distribution inside the

cavity is highly dependent on the forced convection flow caused by movement of the lids. In the next figure Richardson number is assumed to be equal to unity which is for pure mixed convection and a similar pattern is observed in this case except that the isotherms near the side walls become sharper. The upper figure of 3.7(a) is for Ri = 10 which is for free convection dominated region. The temperature distribution in this case is almost opposite of the other two case since natural convection is dominant in this case. It is also visible that the isothermal lines are in upward direction.

In the figure 3.7(b) the streamlines for various Ri is observed. Ri = 0 is for pure forced convection which occurs due to the movement of the lids and thus, the formed vortices are due to the forced convection. A similar distribution is observed for Ri = 1. For Ri = 10, a visible change is found compared to the previous two cases. Effect of natural convection and the force caused by the upper lid reinforce each other, thus a powerful vortex is formed which occupies bulk of the cavity. The previously existing vortices are closer to the side walls and two new vortices are formed near the heat generating object which illustrates the increment in the velocity of the fluid. Again the heatlines for various values of Richardson number is shown in the figure 3.7(c) while the other parameters are Pr = 6.2, Re = 100, Q = 1, K = 5 and χ = 0.05. For these three cases there are well built effect of increasing values Ri. For pure forced convection (Ri = 0) and pure mixed convection (Ri = 1) the heatlines are condensed near the heat generating object and gradually they are transmitting heat to the nearby cold side walls. For Ri = 10 which is for free convection region, the heatlines spread over the whole region. In this case the heatflux magnitude is very high near the solid body which is the region for natural convection.

Figure 3.7: (a) Isotherms, (b) streamlines and (c) heatlines (case I) for different values of Ri with Pr = 6.2, Re = 100, Q = 1, K = 5 and χ = 0.05.

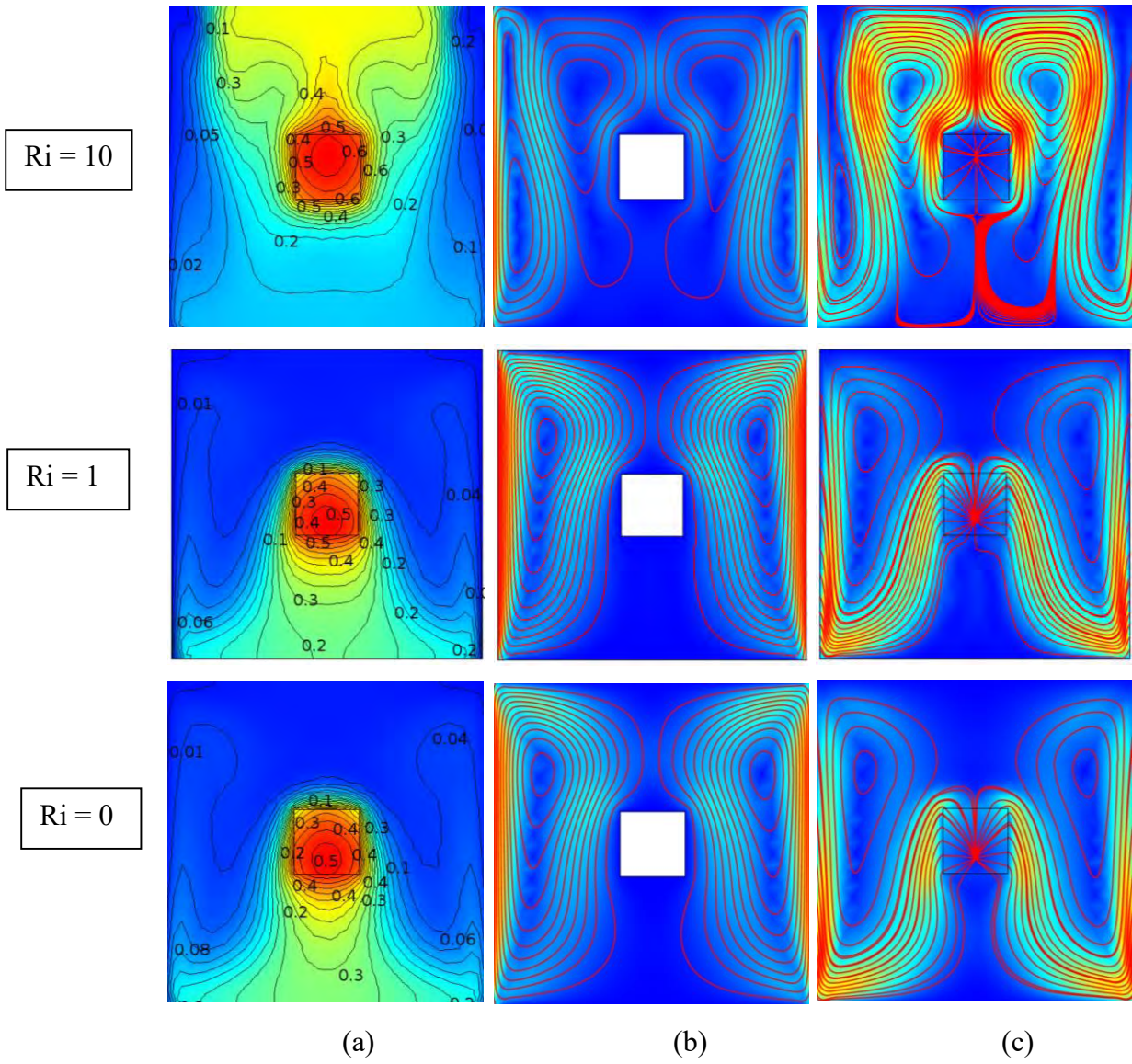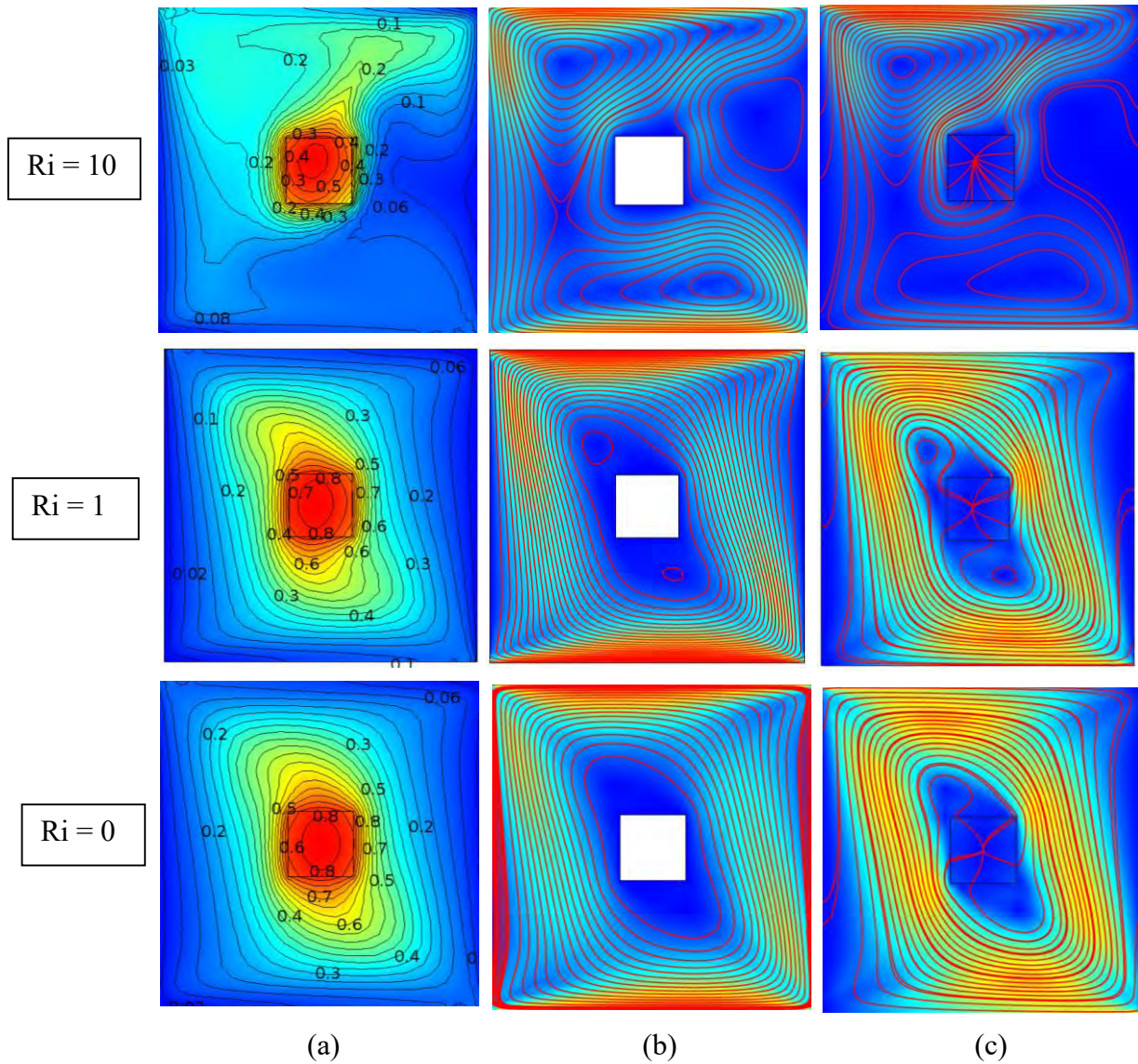**Figure 3.8:** (a) Isotherms, (b) streamlines and (c) heatlines (case II) for different values of Ri, with Pr = 6.2, Re = 100, Q = 1, K = 5 and χ = 0.05.

In the figure 3.8, the isotherms, streamlines and heatlines are represented in terms of various Richardson number for case II where the upper lid is moving left and lower lid is moving right at a constant velocity and the other parameters are kept fixed as Pr = 6.2, Re = 100, Q = 1, K = 5 and χ = 0.05. In figure 3.8(a), isotherms for different Ri are shown. When Ri = 0, this means that the force due to movement of the lids dominates. Isotherms near the heat generating object are higher valued and near the side walls are lower valued. The flow pattern is strongly affected by the movement of the upper and lower lids. That is why the shape of the isothermal lines are rectangular near the side walls and elliptic at the center of the cavity. The case Ri = 1 is for pure mixed convection the flow pattern is almost similar to the previous case. Again the third case is for Ri = 10 which means free convection dominates over the cavity and mentionable difference is observed than the other two cases. The isothermal lines are towards the right corner. In the figure 3.8(b) streamlines are shown and the fluid flow is widely affected by the increasing value of Richardson number. For Ri = 0 and Ri = 1, the flow pattern follows the same direction which occurs due to the movement of the upper and lower lids. Number of streamlines increase for the second case and both of them are in counterclockwise direction since the upper lid is moving left and lower lid is moving right. At Ri = 10 which is the case of free convection and thus a more powerful primary vortex than the previous cases is formed. It is observed that additional vortices are formed at Ri = 10. In figure 3.8(c) heatlines are shown for Ri = 0, 1 and 10. For the first two cases that is for Ri = 0 and Ri = 1, the heat transfer rate is almost similar which happens for the case of lower Richardson number. The third figure is set for Ri = 10, thus the buoyancy force is dominant and additional vortex is formed and heat transfer rate increases due to the buoyancy force. In figure 3.9, average Nusselt number on the heated surface, average temperature of the solid and fluid, maximum temperature of the solid and fluid and average heat flux magnitude for various Richardson number are shown for case I and II.

(a)

(b)

(c)

(d)
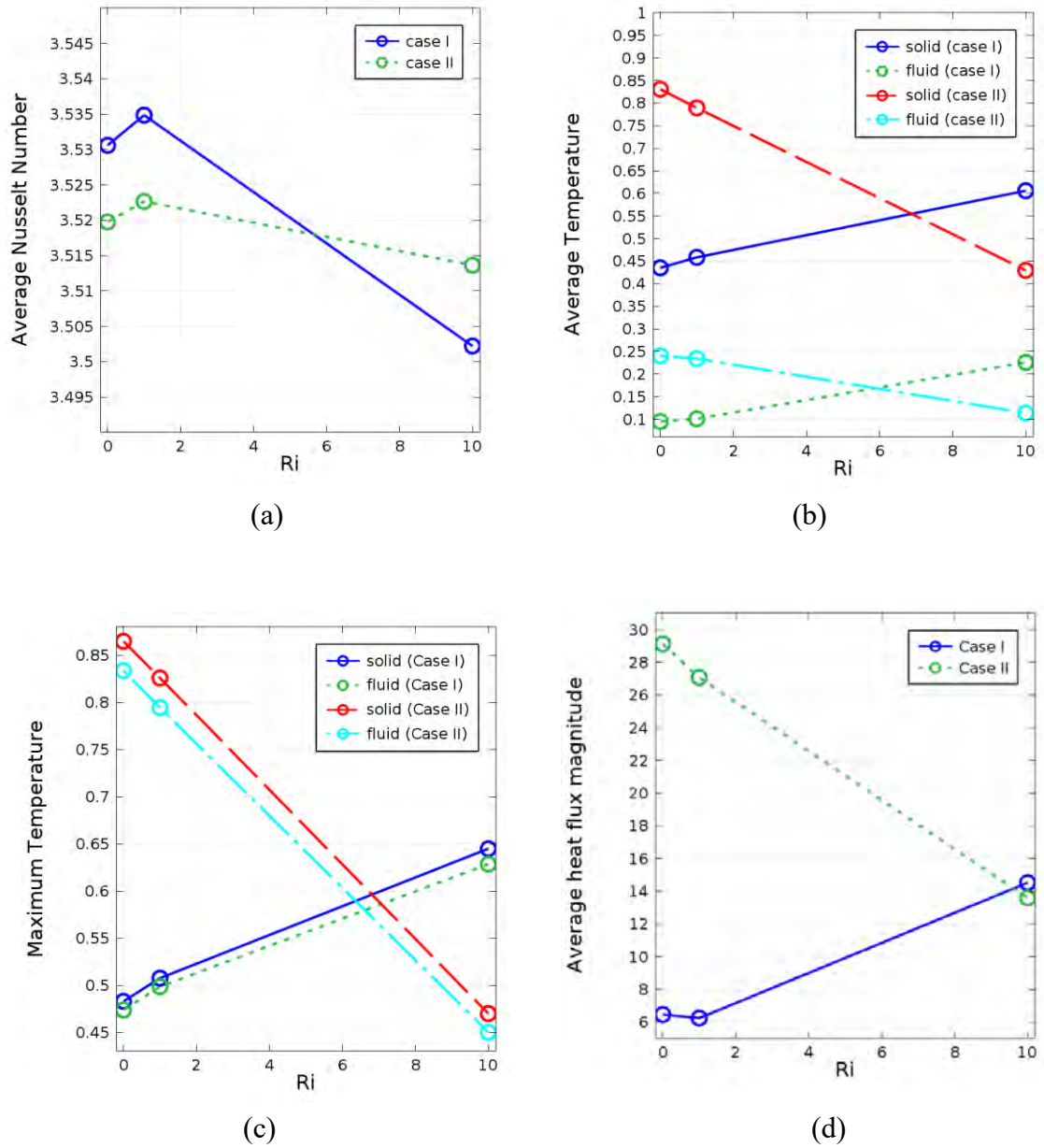
Figure 3.9: (a) Average Nusselt number, (b) average temperature of the solid and the fluid, (c) maximum temperature of the solid and the fluid and (d) average heat flux magnitude for different values of Ri, with $Pr = 6.2$, $Re = 100$, $Q = 1$, $K = 5$ and $\chi = 0.05$.

Table 3.3 (a): Variation of average Nusselt number with Ri

Ri	Case I	Case II
0	3.53060	3.51977
1	3.53487	3.52266
10	3.50223	3.51366

Table 3.3 (b): Variation of average temperature with Ri

Ri	solid(case I)	fluid(case I)	solid(case II)	fluid(case II)
0	0.43522	0.09489	0.83076	0.24024
1	0.45835	0.10063	0.78946	0.23397
10	0.60597	0.22565	0.42951	0.11348

Table 3.3 (c): Variation of maximum temperature with Ri

Ri	solid(case I)	fluid(case I)	solid(case II)	fluid(case II)
0	0.48301	0.47385	0.8649	0.83378
1	0.50766	0.49863	0.82599	0.79465
10	0.64492	0.62854	0.47006	0.45028

Table 3.3 (d): Variation of average heat flux magnitude with Ri

Ri	Case I	Case II
0	6.46974	29.13694
1	6.24818	27.07513
10	14.5294	13.5932

The first figure is for average Nusselt number vs. Ri which shows that when Ri increases from 0 to 1, then the average Nusselt number increases and when Ri increases from 1 to 10 then average Nusselt number decreases for case I. The heat decreases fast for case I. for case II similarity is found as case I. The next figure is for average temperature of the solid and fluid. The average temperature for solid and fluid increases for case I and decreases for that of case II. Also the fluid temperature increases for case I and decreases for case II. Again the maximum temperature of solid increases for case I and decreases for case II, maximum temperature of the fluid increases for case I and decreases for case II. Finally the average heat flux magnitude increases for case I and decreases for case. Overall it is clear the all the above mentioned parameters give higher values for case I and comparatively lower values for case II. All the above mentioned results are shown quantitatively in the tables 3.3 (a), (b), (c) and (d).

3.4 Effect of Heat Generation Parameter

Figure 3.10 shows the results obtained for case I in the form of isotherms, streamlines and heatlines for various values of heat generation parameter. For case 1, the upper and lower lids are adiabatic, left and right walls are moving upwards while the other parameters are kept fixed as Pr = 6.2, Re = 100, Ri = 1, K = 5 and χ = 0.05. In figure 3.10(a) the effect on isothermal lines are shown for various Q. Here the red color in the figure indicates the higher temperature and blue color means the lower temperature. For Q = 1 the higher valued isotherms are near the heat generating object and those are elliptic and the isotherms near the moving walls are lower valued which are in parabolic shape. When Q = 2 same pattern is observed like Q = 1. For both cases the flow pattern is uniform on the both sides of the heat generating block. When the value of Q increases, the uniform distribution is devastating and fluctuation in the isothermal lines are observed since the value of the heat generation parameter increases. The isothermal lines are gathering near the right down corner for Q =3 which is more clear for Q = 4. In figure 3.10 (b) the effect on streamlines lines are shown for various Q for case I. Two vortex are formed due to the movement of

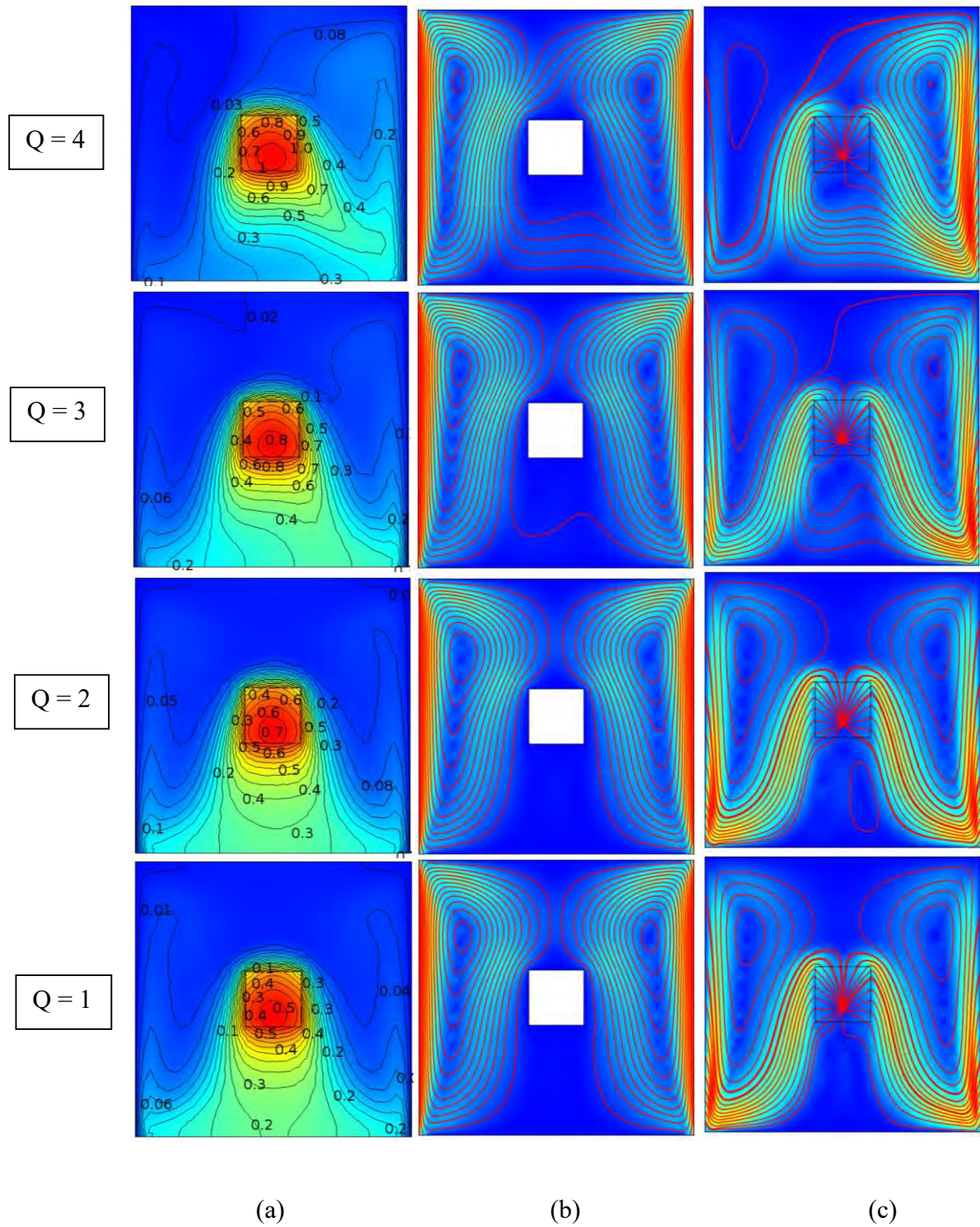**Figure 3.10:** (a) Isotherms, (b) streamlines and (c) heatlines (case I) for different values of Q with Pr = 6.2, Re = 100, Ri = 1, K = 5 and χ = 0.05.
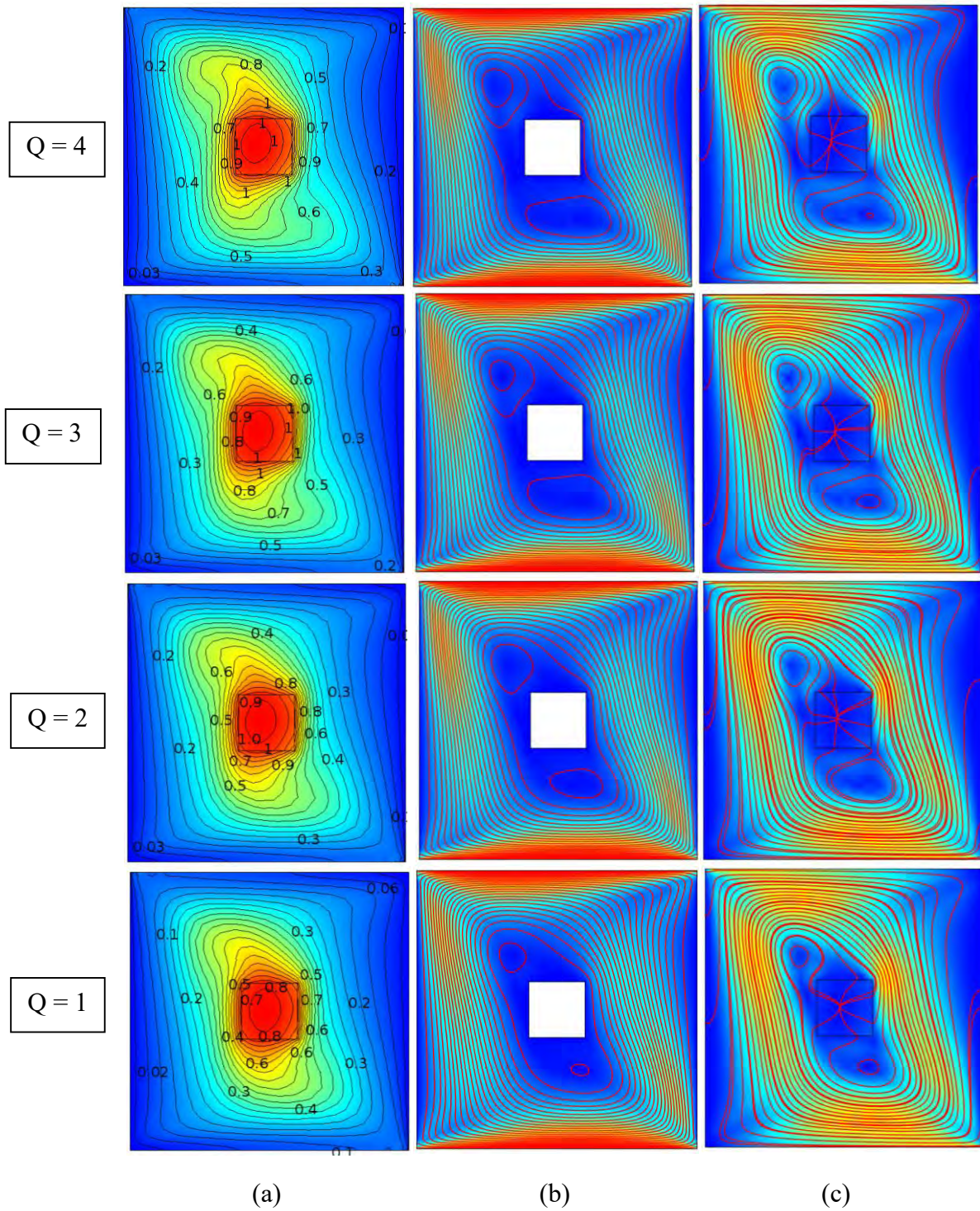
Figure 3.11: (a) Isotherms, (b) streamlines and (c) heatlines (case II) for different values of Q with Pr = 6.2, Re = 100, Ri = 1, K = 5 and χ = 0.05.

the side walls for Q = 1 and Q = 2. At the low heat generation the streamlines are in a clockwise direction near the left wall and in anticlockwise direction near the right wall. The velocity of the fluid is well distributed. For Q = 3 a small disturbance is observed in the streamline pattern which increases for Q = 4 which occurs due to the convection dominant inside the cavity. For Q = 4 the streamlines are nearer the left wall. In figure 3.10 (c) the effect on heatlines lines are shown for various Q. for Q = 1, the heatlines are nearer the heat generating object and elliptic heatlines are near the side vertical walls. For Q = 2 the heatlines pattern remain same. For Q = 3 the heatlines from the left wall are flowing rightward. That is why the heatlines are close to the right wall.Figure 3.11 shows the results obtained for case II in the form of isotherms, streamlines and heatlines for various values of heat generation parameter Q. For case II the upper lid is moving left and lower lid is moving right. Figure 3.11 (a) shows the isothermal lines in the cavity for Q = 1, 2, 3 and 4. For Q = 1, the higher valued isothermal lines are near the heat generating object and the higher valued isothermal lines are near the side walls. At the center the isothermal lines are elliptic and near the side walls those are rectangular which is affected by the movement of the upper and lower lids. The orientation and values of the isothermal lines are almost same for Q = 2. For the values Q =3 and 4, the lines are not that much uniform because heat generation is high in this two cases. In the figure 3.11 (b) the streamlines are shown and it can be said that the flow pattern and strength are almost similar for different values of Q. In the figure 3.11 (c) the heatlines are shown for the case II. The heatlines are circulated around the heat generating object and they are stronger near the moving walls. Therefore it can be concluded from the above discussion that the variation of Q has small effect on case II whether strong effect is observed for case I.

In figure 3.12, average Nusselt number on the heated surface, average temperature of the solid and the fluid, maximum temperature of the solid and the fluid and average heat flux magnitude for various Q are shown for case I and II. For both the cases average Nusselt number increases linearly with the increasing value of Q which indicates that the heat transfer rate increases. Average temperature of the solid and fluid also increase for case I and II. The average temperature for solid and fluid are higher in case II than the values

(a)

(b)

(c)

(d)
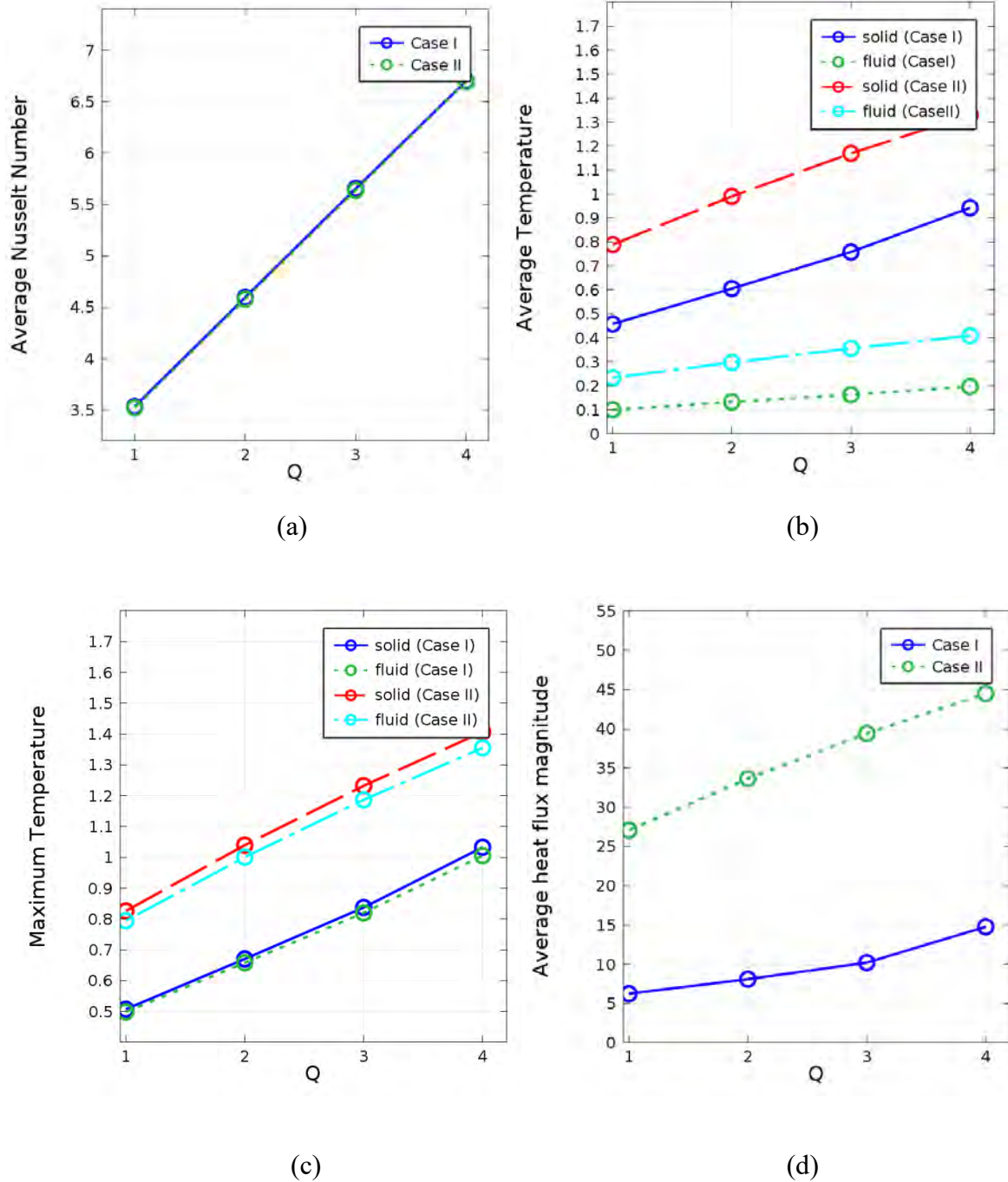
Figure 3.12: (a) Average Nusselt number, (b) average temperature of the solid and the fluid, (c) maximum temperature of the solid and the fluid and (d) average heat flux magnitude for different values of Q with Pr = 6.2, Re = 100, Ri = 1, K = 5 and χ = 0.05.

Table 3.4 (a): Variation of average Nusselt number with Q

Q	Case I	Case II
1	3.53487	3.52261
2	4.59607	4.58001
3	5.6543	5.63713
4	6.70234	6.69514

Table 3.4 (b): Variation of average temperature with Q

Q	solid(case I)	fluid(case I)	solid(case II)	fluid(case II)
1	0.45832	0.10059	0.78707	0.23218
2	0.60610	0.13294	0.99057	0.29786
3	0.75856	0.16319	1.16984	0.35648
4	0.94308	0.19735	1.33053	0.40921

Table 3.4 (c): Variation of maximum temperature with Q

Q	solid(case I)	fluid(case I)	solid(case II)	fluid(case II)
1	0.50758	0.49855	0.82599	0.79466
2	0.67053	0.65824	1.03965	1.00078
3	0.83739	0.82007	1.23240	1.18682
4	1.03293	1.00546	1.40698	1.35535

Table 3.4 (d): Variation of average heat flux magnitude with Q

Q	Case I	Case II
1	6.24505	26.83165
2	8.09123	33.65569
3	10.19957	39.41748
4	14.77178	44.49916

obtained in case I. The maximum temperature for solid and fluid for case I are in increasing approach and the values are close to each other. Similar approach is found in case II and also all the values in case II are higher than case I. The average heat flux magnitude is very high in case II than case I. All the above mentioned results are shown quantitatively in the tables 3.4 (a), (b), (c) and (d).

3.5 Effect of Solid Volume Fraction

Figure 3.13 shows the results obtained for case I in the form of isotherms, streamlines and heatlines for various solid volume fraction. For case 1, the upper and lower lids are adiabatic, left and right walls are moving upwards while the other parameters are kept fixed as Pr = 6.2, Re = 100, K = 5, Ri = 1 and Q = 1. Here the effect of the solid volume fractions is investigated in the range of 0% – 10%. The isotherms for various solid volume fraction of nano particle inside a double lid driven cavity with a square heat generating block are shown in figure 3.13(a). From the figure it can be said that the solid volume fraction of nano particle effects significantly on isotherm structure. If the solid volume fraction is 0% that is for normal fluid isotherms are parabolic near the heat generating block. If solid volume fraction χ is increased from 0% to 10% then the parabolic shaped isotherms increase. Making a comparison of the isotherm lines for various solid volume fractions, the isotherms are slightly shifted from the heat generating block to the side wall. The flow field inside a double lid driven cavity with heat generating object in terms of computed streamlines for various solid volume fraction χ is shown in figure 3.13(b). The size of the vortex as well as the flow strength has a small effect as the solid volume fraction is increased from 0% to 10%. For the given boundary condition there forms a counter clockwise vortex inside the cavity. If the solid volume fraction χ is increased the vortex inside the cavity becomes slightly weaker. The heat lines for various solid volume fraction χ are shown in figure 3.13(c). From the figure it can easily be said that there is less effect of solid volume fraction χ on heat line structure. When the solid volume fraction χ is 0% that is in absence of nano particles then the heat flux lines are circulating from the center

χ = 0.1

χ = 0.05

χ = 0.02

χ = 0

(a) (b) (c)

Figure 3.13: (a) Isotherms, (b) streamlines and (c) heatlines (case I) for different values of χ with Pr = 6.2, Re = 100, K = 5, Ri = 1 and Q = 1.

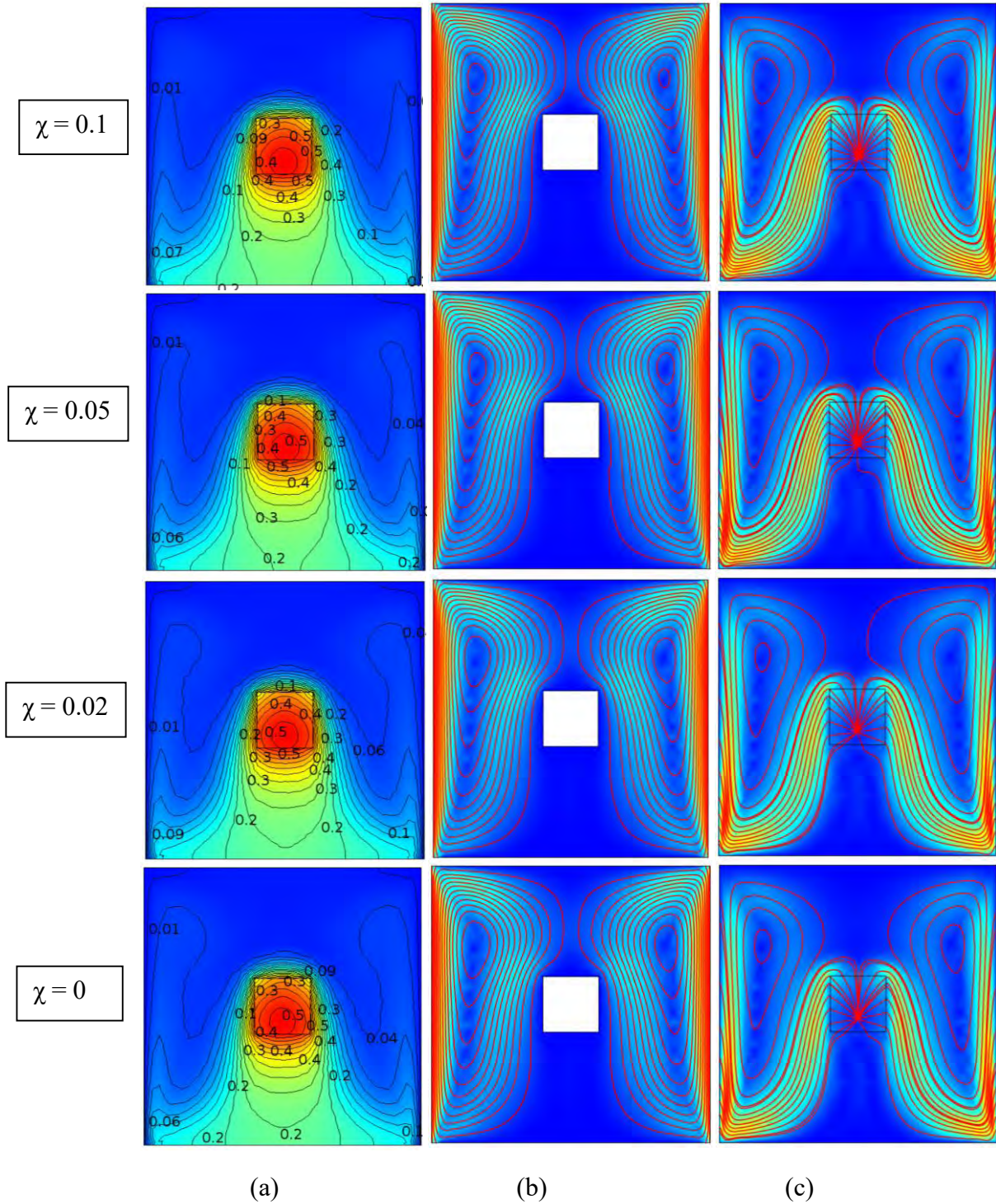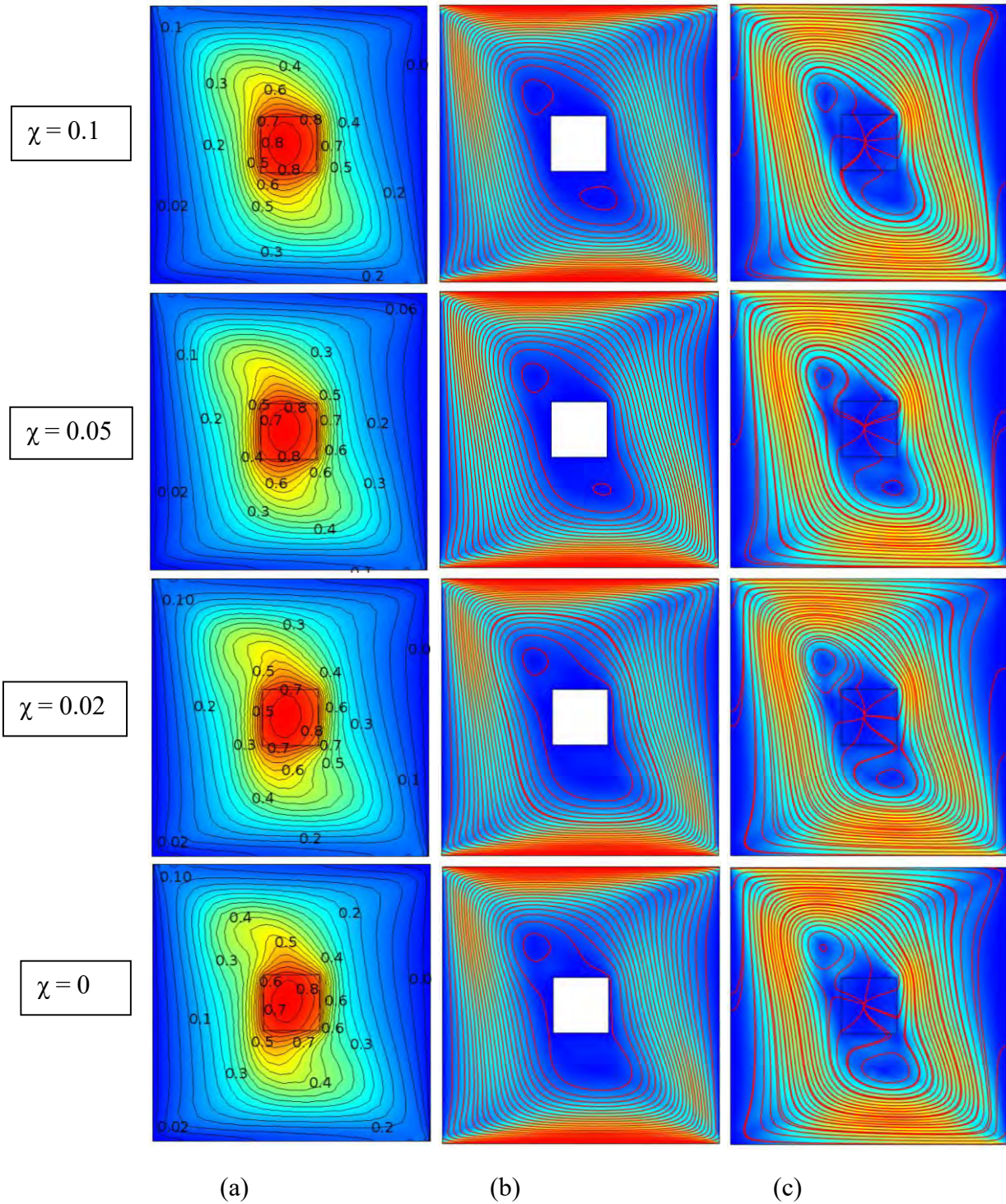**Figure 3.14:** (a) Isotherms, (b) streamlines and (c) heatlines (case II) for different values of χ with Pr = 6.2, Re = 100, K = 5, Ri = 1 and Q = 1.

towards the side walls which occurs due to the movement of the walls. When the solid volume fraction is increased it is observed that the density of circulations also increases. Since alumina has relatively high thermal conductivity when the solid volume fraction χ is increased then the heat flow also increases. The trajectory of the heat flow is nearer to the moving side walls. In the figure 3.14 results are obtained for case II in the form of isotherms, streamlines and heatlines for various solid volume fraction χ keeping the other parameter fixed as Pr = 6.2, Re = 100, K = 5, Ri = 1 and Q = 1. Isotherms for different values of solid volume fraction for case II are shown in figure 3.14(a). The isothermal lines are elliptic near the block and rectangular near the side walls. The higher valued isothermal lines are near the heat generating block and the lower valued lines are near the boundaries when χ = 0. The flow pattern remains the same as the previous value of χ for the other values like χ = 0.02, χ = 0.05 and χ = 0.1 when the property of the working fluid is changed. The flow field inside a double lid driven cavity with heat generating object in terms of computed streamlines for various solid volume fraction χ is shown in figure 3.14(b) for the second case. The size of the vortex as well as the flow strength has a small effect as the solid volume fraction is increased from 0% to 10%. For the given boundary condition there forms a counter clockwise vortex inside the cavity. If the solid volume fraction χ is increased the vortex inside the cavity becomes slightly weaker. The heat lines for various solid volume fraction χ are shown in figure 3.14(c). When solid volume fraction increases from 0% to 10%, the heatlines are denser significantly due to the presence of nano particles.

In figure 3.15, average Nusselt number on the heated surface, average temperature of the solid and the fluid, maximum temperature in the cavity and average heat flux magnitude for various χ are shown for case I and II. For both the cases average Nusselt number increases linearly with the increasing value of χ which indicates that the heat transfer rate increases. Average temperature of the solid and fluid also increase slowly for case I and II. The average temperature for solid and fluid are higher in case II than the values obtained in case I. The maximum temperature for solid and fluid for case I are in increasing approach and the values are close to each other. Average heat flux magnitude decreases for the increasing values of χ. All the above mentioned results are shown quantitatively in the tables 3.5 (a), (b), (c) and (d).

(a)

(b)

(c)

(d)
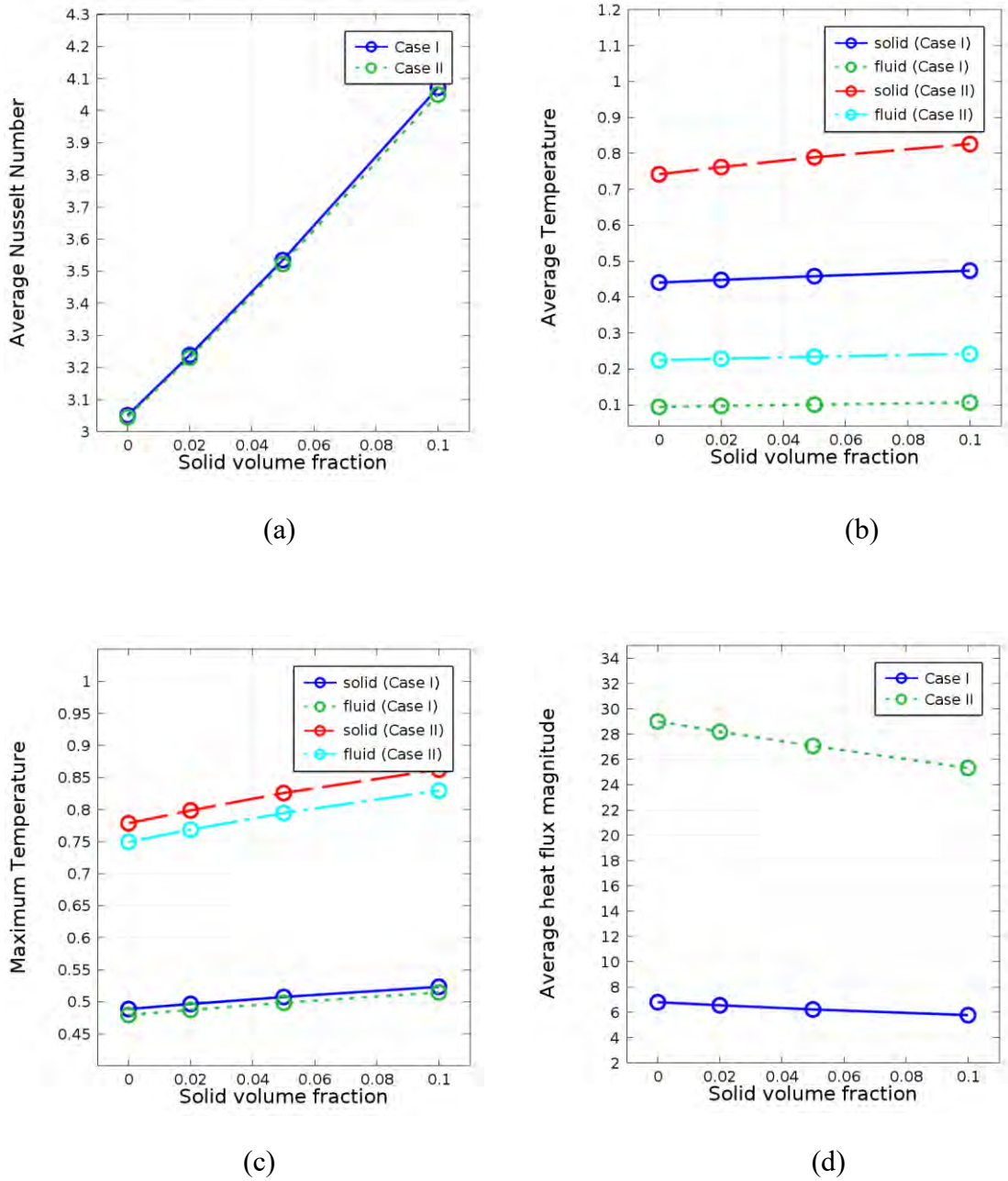
Figure 3.15: (a) Average Nusselt number, (b) average temperature of the solid and the fluid, (c) maximum temperature of the solid and the fluid and (d) average heat flux magnitude for different values of χ, with Pr = 6.2, Re = 100, K = 5, Ri = 1 and Q = 1.

Table 3.5 (a): Variation of average Nusselt number with χ

X	Case I	Case II
0	3.05133	3.04544
0.02	3.23885	3.23099
0.05	3.53487	3.52261
0.1	4.07147	4.05006

Table 3.5 (b): Variation of average temperature with χ

χ	solid(case I)	fluid(case I)	solid(case II)	fluid(case II)
0	0.44053	0.0942	0.74216	0.22416
0.02	0.44795	0.09683	0.76214	0.22834
0.05	0.45832	0.10059	0.78707	0.23218
0.1	0.47372	0.1064	0.82627	0.24191

Table 3.5 (c): Variation of maximum temperature with χ

X	solid(case I)	fluid(case I)	solid(case II)	fluid(case II)
0	0.48889	0.47950	0.77873	0.74974
0.02	0.49675	0.48752	0.79873	0.76881
0.05	0.50763	0.4986	0.82604	0.79471
0.1	0.52353	0.5147	0.86251	0.82984

Table 3.5 (d): Variation of average heat flux magnitude with χ

X	Case I	Case II
0	6.81915	29.01325
0.02	6.57152	28.208685
0.05	6.24505	26.83165
0.1	5.79367	25.34469

Finally the variation of average Nusselt number and average heat flux magnitude for the different values of Reynolds number Re, solid fluid thermal conductivity ratio K, Richardson number Ri, heat generation parameter Q and solid volume fraction χ for case I and II are shown in the table 3.6 and 3.7.

Table 3.6: Variation of average Nusselt number

Re	K	Ri	Q	χ	Case I	Case II
20	5	1	1	0.05	3.53386	3.51295
50	5	1	1	0.05	3.53180	3.52286
100	5	1	1	0.05	3.53487	3.52267
150	5	1	1	0.05	3.53455	3.51710
100	0.2	1	1	0.05	15.86172	15.93062
100	1	1	1	0.05	5.92333	5.95942
100	5	1	1	0.05	3.53487	3.52261
100	50	1	1	0.05	2.80057	2.79524
100	5	0	1	0.05	3.53060	3.51977
100	5	1	1	0.05	3.53487	3.52266
100	5	10	1	0.05	3.50223	3.51366
100	5	1	1	0.05	3.53487	3.52261
100	5	1	2	0.05	4.59607	4.58001
100	5	1	3	0.05	5.6543	5.63713
100	5	1	4	0.05	6.70234	6.69514
100	5	1	1	0	3.05133	3.04544
100	5	1	1	0.02	3.23885	3.23099
100	5	1	1	0.05	3.53487	3.52261
100	5	1	1	0.1	4.07147	4.05006

Table 3.7: Variation of average heat flux magnitude.

Re	K	Ri	Q	χ	Case I	Case II
20	5	1	1	0.05	3.60620	8.96568
50	5	1	1	0.05	4.73351	16.6571
100	5	1	1	0.05	6.24679	27.0822
150	5	1	1	0.05	7.82795	34.43532
100	0.2	1	1	0.05	6.08861	27.06434
100	1	1	1	0.05	6.13194	26.79185
100	5	1	1	0.05	6.24505	26.83165
100	50	1	1	0.05	6.35479	27.11632
100	5	0	1	0.05	6.46974	29.13694
100	5	1	1	0.05	6.24818	27.07513
100	5	10	1	0.05	14.5294	13.5932
100	5	1	1	0.05	6.24505	26.83165
100	5	1	2	0.05	8.09123	33.65569
100	5	1	3	0.05	10.19957	39.41748
100	5	1	4	0.05	14.77178	44.49916
100	5	1	1	0	6.81915	29.01325
100	5	1	1	0.02	6.57152	28.20869
100	5	1	1	0.05	6.24505	26.83165
100	5	1	1	0.1	5.79367	25.34469

It is found from the table 3.6 the heat transfer rate is maximum for Re = 100, K = 0.2, Ri = 1, Q = 1 and χ = 0.05 for both cases. Also it is observed from table 3.7 that the average heat flux magnitude is maximum for Re = 100, K = 5, Ri = 1, Q = 4 and χ = 0.05 for case I and case II but case II gives much higher value than that of case I.

CHAPTER 4
CONCLUSIONS

Mixed convection in a lid driven cavity containing a heat generating object using water-alumina (Al_2O_3) nanofluids under the influence of heatlines has been investigated numerically. The results are presented for flow and thermal fields as well as heat transfer inside the cavity. In this thesis paper two cases are considered, (i) two vertical moving walls while the remaining sidewalls are kept adiabatic and (ii) two horizontal walls moving towards opposite direction and the heat generating object is placed at the center of the cavity. Finite element method is used to solve governing equations. Comparisons with the beforehand published work are performed and found to be in excellent agreement. The effect of different dimensionless parameters like Reynolds number (Re), Solid fluid thermal conductivity ratio (K), the Richardson number (Ri), heat generation parameter (Q) and solid volume fraction (χ) have been reported. The various ideas and results have been discussed in detail in the relevant chapters of the thesis. In the present chapter an attempt is made to summarize the concepts presented and results obtained in the work reported already. A section on the scope of further work on associated fields of investigation is also included.

4.1 Summery of the Major Outcomes

The analysis has been confined to case of lid driven cavity containing heat generating block exerting constant heat flux. The nature of flow and thermal fields and the characteristics of heat transfer process particularly its augmentation due to the presence of nanofluid in the cavity is discussed in chapter 3 and the results are shown in terms of isotherms, streamlines and heatlines. Two different cases were under consideration depending on the movement of any two side walls and keeping the remaining two walls adiabatic. The effect of the dimensionless parameters such as Reynolds number (Re), solid fluid thermal conductivity ratio (K), the Richardson number (Ri), heat generation parameter (Q) and solid volume

fraction (χ) are analyzed for both the cases in details in the previous chapter. On the basis of the analysis the following conclusions have been drawn:

(i)   There is notable effect of Re on isotherms, streamlines and heatlines for both considered cases. For the increasing values of Re, little change is observed in the average Nusselt number, the values obtained for case I are higher than that of case II. Average heat flux magnitude increases rapidly for case II while the values for case I increases slowly for the increment of Re.

(ii)   In general the solid fluid thermal conductivity ratio K has a strong influence on thermal fields but there is a negligible effect on streamlines for the increasing values of K. For both cases, average Nusselt number decreases rapidly when K changes from 0.2 to 5 and decreases very slowly from 5 to 50. Again for the variation of K there is negligible effect on heat flow while case II gives higher value than case I.

(iii)   There is significant effect on isothermal lines, streamlines and heatlines. For both cases when Ri = 0 and 1, the thermal and flow field have similar pattern whose change is noticeable for Ri = 10. Heat transfer rate increases when mode of convection is changed from forced to mixed convection and decreases when it is changing from mixed to free convection. Again heat flux magnitude changes differently for case I and case II.

(iv)   The effect on isotherms is remarkable for the variation of Q from 1 to 4 but streamlines and heatlines are not that much affected. The average Nusselt number, average temperature of the solid and fluid, maximum temperature of the solid and fluid and average heat flux magnitude all increase for the increasing values of Q. The flux magnitude is higher for case II than case I but the heat transfer rate is almost same for both cases which increases linearly for the increasing values of Q.

(v)   There is mild effect on the flow field if the solid volume fraction increases from 0%-10%. If χ increases then the heat transfer rate increases. Average Nusselt number increases vary rapidly, average temperature and maximum temperature for solid and fluid increases slowly and average heat flux magnitude decreases for the increasing value of χ.

(vi)   Though the heat flow is higher in case II than case I but there is no significant change in heat transfer rate for the two considered cases. Better heat transfer rate can be achieved for higher values of Re, Q, χ and lower values of K at Ri = 1.

4.2 Further Works

The following can be put forward for the further works as follow-ups of the present research as.

- Double diffusive mixed convection can be analyzed through including the governing equation of concentration conservation.

- Investigation can be performed by using magnetic fluid instead of electrically conducting fluid within the porous medium and changing the boundary conditions of the cavity's walls.

- Only two-dimensional fluid flow and heat transfer has been analyzed in this thesis. So this deliberation may be extended to three-dimensional analyses to investigate the effects of parameters on flow fields and heat transfer in cavities. The study can be extended for another nanofluid other than Al_2O_3 so that the results can be compared for better one.

- Single phase flow model is considered. Two phase models may be analyzed and compared to the single phase model.

REFERENCES:

[1]   Aminossadati, S. M., and Ghasemib, B., "A Numerical Study of Mixed Convection in a Horizontal Channel with a Discrete Heat Source in an Open Cavity", European Journal of Mechanics-B/Fluids, Vol. 28, No. 4, pp. 590-598, 2009.

[2]   Aydin, O., and Yang, W. J., "Mixed Convection in Cavities with a Locally Heated Lower and Moving Side Walls", Numerical Heat Transfer, Part A, Vol. 37, pp. 695-710, 2000.

[3]   Basak T., Roy, S., Singh, S. K., and Pop, I., "Analysis of Mixed Convection in a Lid-Driven Porous Square Cavity with Linearly Heated Side Wall(s)", International Journal of Heat and Mass Transfer, Vol. 53, pp. 1819–1840, 2010.

[4]   Beck, M. P., Sun, T., and Teja, A. S., "The Thermal Conductivity of Alumina Nanoparticles Dispersed in Ethylene Glycol", Fluid Phase Equilibria, Vol. 260, No. 2, pp. 275-278, 2007.

[5]   Bello-Ochenda, F. L., "A Heat Function Formulation for Thermal Convection in a Square Cavity", International Communications in Heat and Mass Transfer, Vol. 15, pp. 193-202, 1988.

[6]   Billah, M. M., Rahman, M. M., Kabir, M. H., and Uddin M. Sharif, "Heat Transfer and Flow Characteristic for MHD Mixed Convection in a Lid Driven Cavity with Heat Generating Obstacle", International Journal of Energy & Technology 3, Vol. 32, pp. 1-8, 2011.

[7]   Brinkmann, H. C., "The Viscosity of Concentrated Suspensions and Solutions", The Journal of Chemical Physics, Vol. 20, No. 4, pp. 571, 1952.

[8]   Chamkha, A. J., Hussain, S. H., and Abd-Amer, Q. R., "Mixed Convection Heat Transfer of Air inside a Square Vented Cavity with a Heated Horizontal Square Cylinder.", Numerical Heat Transfer, Part A, Vol. 59, No.1, pp. 58-79, 2011.

[9]   Chamkha, A. J., Ismael, M. A., and Pop, I., "Mixed Convection in a Lid-Driven Square Cavity with Partial Slip", International Journal of Thermal Sciences, Vol. 82, pp. 47 – 61, 2014.

[10]   Chandrasekar, M., Suresh, S., and Bose, A. C., "Experimental Investigations and Theoretical Determination of Thermal Conductivity and Viscosity ofAl_2O_3/water Nanofluid", Experimental Thermal and Fluid Science, Vol. 34, No. 2, pp. 210-216, 2010.

[11]   Chen, H., Ding, Y., and Lapkin, A., "Rheological Behavior of Nanofluids Containing Tube/Rode-Like Nanoparticles", Powder Technology, Vol. 194, pp. 132-141, 2009.

[12]   Choi, S. U. S., "Nanofluids: From Vision to Reality through Research", Journal of Heat Transfer, Vol. 131, pp. 033106-033109, 2009.

[13]   Colangelo, G., Favale, E., de Risi, A., and Laforgia, D., "Results of Experimental Investigations on the Heat Conductivity of Nanofluids Based on Diathermic Oil for High Temperature Applications", Applied Energy, Vol. 97, pp. 828-833, 2011.

[14]   Corcione, M., "Empircal Correlating Equations for Predicting the Effective Thermal Conductivity and Dynamic Viscosity of Nanofluids", Energy Conversion and Management, Vol. 52, No. 1, pp. 789-793, 2011.

[15]   Corcione, M., "Heat Transfer Features of Buoyancy-Driven Nanofluids inside Rectangular Enclosures Differentially Heated at the Sidewalls", International Journal of Thermal Sciences, Vol. 49, pp.1536-1546, 2010.

[16]   Costa, V. A. F., "Heatline and Massline Visualization of Laminar Natural Convection Boundary Layers near a Vertical Wall", International Journal of Heat and Mass Transfer, Vol. 43, No. 20, pp. 3765-3774, 2000.

[17]   Dalal, A., and Das, M. K., "Heatline Method for the Visualization of Natural Convection in a Complicated Cavity", International Journal of Heat and Mass Transfer, Vol. 51, No. 1-2, pp. 263–272, 2008.

[18]   Deng, Q. H., and Tang, G. F., "Numerical Visualization of Mass and Heat Transport for Conjugate Natural Convection/Heat Conduction by Streamline and Heatline,", International Journal of Heat and Mass Transfer, Vol. 45 ,No. 11, pp. 2373–2385, 2002.

[19]   Esfe, M. H., Ghadi, A. Z., and Noroozi, M. J., "Numerical Simulation of Mixed Convection within Nanofluid Filled Cavities with Two Adjacent Moving Walls", Transactions of the Canadian Society for Mechanical Engineering, Vol. 37, No. 4, pp. 1073-1083, 2013.

[20]   Fatih, S., "Numerical Analysis and POD based Interpolation of Mixed Convection Heat Transfer in Horizontal Channel with Cavity Heated from Below", Transactions of the Canadian Society for Mechanical Engineering, Vol. 7, No. 2, pp. 261-271, 2013.

[21]   Gau, G., and Sharif, M. A. R., "Mixed Convection in Rectangular Cavities at Various Aspect Ratios with Moving Isothermal Side Walls and Constant Flux Heat Source on the Bottom Wall", International Journal of Thermal Sciences, Vol. 43, pp. 465-475, 2004.

[22]   Hasib, M. H., Saha, S., Hossen, S., and Saha, S. C., "Onset of Transition in Mixed Convection of a Lid-Driven Trapezoidal Enclosure Filled with Water-Al2O3 Nanofluid", Proceedings of the 19th Australasian Fluid Mechanics Conference, RMIT University Melbourne, Australia, pp. 177, 2014.

[23]   Khanafer, K., Vafai, K., and Lightstone, M., "Mixed Convection Heat Transfer in Two-Dimensional Open-Ended Enclosure", International Journal of Heat and Mass Transfer, Vol. 45, pp. 5171-5190, 2002.

[24]   Kimura, S., and Bejan, A., "The Heatline Visualization of Convective Heat Transfer, Journal of Heat Transfer" Vol. 105, pp. 916-919, 1983.

[25]   Leong, J. C., Brown, N. M., and Lai, F. C., "Mixed Convection from an Open Cavity in a Horizontal Channel", International Communications in Heat and Mass Transfer, Vol. 32, pp. 583-592, 2005.

[26]   Luo, W. J., and Yang, R. J., "Multiple Fluid Flow and Heat Transfer Solutions in a Two-sided Lid Driven Cavity", International Journal of Heat and Mass Transfer, Vol. 50, pp. 2394-2405, 2007.

[27]   Mahapatra, P. S., Mukhopadhyay, A., Manna, N. K., and Ghosh, K., "Heatlines and other Visualization Techniques for Confined Heat Transfer Systems", International Journal of Heat and Mass Transfer, Vol. 118, pp. 1069 - 1079, 2018.

[28]   Manca, O., Nardini, S., and Vafai, K., "Experimental Investigation of Mixed Convection in a Channel with an Open Cavity", Experimental Heat Transfer, Vol. 19, pp. 53–68, 2006.

[29]   Manca, O., Nardini, S., Khanafer, K., and Vafi, K., "Effect of Heated Wall Position on Mixed Convection in a Channel with an Open Cavity", Numerical Heat Transfer, Part A, Vol. 43 pp. 259-282, 2003.

[30]   Monsour, S. A., Al-Ghoury, M. E., Shalaan, E., El Eraki, M. H. I., and Abdel-Bary, E. M., "Thermal Properties of Graphite-Loaded Nitrite Rubber/Poly (Vinyl Chloride) Blends", Journal of Applied Polymer Science, Vol. 116, No. 6, pp. 3171-3177, 2010.

[31]   Mukhopadhyay, A., Qin, X., Aggarwal, S. K., and Puri, I. K., "On Extension of Heatline and Massline Concepts to Reacting Flows through Use of Conserved Scalars", Journal of Heat Transfer Transaction, ASME 124, Vol. 4, pp. 791–799, 2002.

[32]   Muthtamilselvan, M., Kandaswamy, P., and Lee, J., "Heat Transfer Enhancement of Copper-water Nanofluids in a Lid-driven Enclosure", Communications in Nonlinear Science and Numerical Simulation, Vol. 15, No. 6, pp. 1501-1510, 2010.

[33]   Nada, E. A., and Chamkha, A. J., "Mixed Convection Fow of a Nanofluid in a Lid-Driven Cavity with a Wavy Wall", International Communications in Heat and Mass Transfer, Vol. 57, pp. 36–47, 2014.

[34]   Nayak R. K., Bhattacharyya S., and Pop I., "Numerical Study on Mixed Convection and Entropy Generation of a Nanofluid in a Lid-Driven Square Enclosure,", Journal of Heat Transfer, Vol. 138, No. 1, pp. 11, 2015.

[35]   Parvin, S., Ahmed. K. F. U., Alim, M. A., and Hossain, N. F., "Heat Transfer Enhancement by Nanofluid in a Cavity Containing a Heated Obstacle", International Journal of Mechanical and Material Engineering, Vol. 7, No. 2, pp. 128-135, 2012.

[36]   Parvin, S., and Siddiqua, A., "Heatline Analysis for MHD Mixed Convection Flow of Nanofluid within a Driven Cavity Containing Heat Generating Block", AIP Conference Proceedings 1754, 050001; doi: 10.1063/1.4958392, 2016.

[37]   Parvin, S., Siddiqua, A., and Elias, M., "Effect of Reynold's Number for Mixed Convection Flow of Nanofluid in a Double Lid Driven Cavity with Heat Generating Obstacle", Heat and Mass Transfer Research Journal, Vol. 1, No. 1, 2017.

[38]   Rahman, M. M., Saidur, R., and Rahim, N. A., "Conjugated Effect of Joule Heating and Magneto-Hydrodynamic on Double-Diffusive Mixed Convection in a Horizontal Channel with an Open Cavity", International Journal of Heat and Mass Transfer, Vol. 54, pp. 3201-3213, 2011.

[39]   Rahman, M. M, Parvin, S, Saidur R., and Rahim, N. A., "Magnetohydrodynamic Mixed Convection in a Horizontal Channel with an Open Cavity", International Communications in Heat and Mass Transfer, Vol. 38, pp. 184-193, 2011.

[40]   Rahman, M. M., Alim, M. A., and Chowdhury, M. K., "Magnetohydrodynamic Mixed Convection Around a Heat Conducting Horizontal Circular Cylinder in a Rectangular Lid-Driven Cavity with Joule Heating", Journal of Scientific Research Vol. 1, No. 3, pp. 461-472, 2009.

[41]   Rahman, M. M., Billah, M. M., Mamun, M. A. H, Saidur, R., and Hasanuzzamaz, M., "Reynolds and Prandtl Numbers Effects on MHD Mixed Convection in a Lid-driven Cavity along with Joule Heating and a Centered Heat Conducting Circular Block", International Journal of Mechanical and Materials Engineering, Vol. 5, No. 2, pp. 163-170, 2010.

[42]   Rahman, M. M., Parvin, S., Hasanuzzamaz, M., Saidur, R., and Rahim, N. A., "Effect of Heat— generating Solid Body on Mixed Convection Flow in a Ventilated Cavity", Heat Transfer Engineering, Vol. 34, pp. 1- 13, 2013.

[43]   Rashidi, M. M., Nasiri, M., Khezerloo, M., and Laraqi, N., "Numerical Investigation of Magnetic Field Effect on Mixed Convection Heat Transfer of Nanofluid in a Channel with Sinusoidal Walls", Journal of Magnetism and Magnetic Materials, Vol. 401, pp. 159-168, 2016.

[44]   Roy, M., Biswal, P., Roy, S., and Basak, T., "Heat Flow Visualization During Mixed Convection within Entrapped Porous Triangular Cavities with Moving Horizontal Walls via Heatline Analysis", International Journal of Heat and Mass Transfer, Vol. 108, pp. 468-489, 2017.

[45]   Sheikholeslami, M., and Rokni, B. H., "Melting Heat Transfer Influence on Nanofluid Flow Inside a Cavity in Existence of Magnetic Field", International Journal of Heat and Mass Transfer, Vol. 114, pp. 517-526, 2017.

[46]   Sheikholeslami, M., Hayat, T., and Alsaedi, A., "MHD free Convection of Al_2O_3-water Nanofluid Considering Thermal Radiation: A Numerical Study", International Journal of Heat and Mass Transfer, Vol. 96, pp. 513-524, 2016.

[47]   Yapici, K., and Obut, S., "Laminar Mixed-Convection Heat Transfer in a Lid-Driven Cavity with Modified Heated Wall". Heat Transfer Engineering, Vol. 36, No. 3, pp. 303–314, 2015.

[48]   Zienkiewicz, O. C., and Taylor, R. L., "The Finite Element Method", Mc-Graw Hill, UK, 1991.